

Substrate induced changes in atomically thin 2-dimensional semiconductors: Fundamentals, engineering, and applications

Yinghui Sun,¹ Rongming Wang,¹ and Kai Liu^{2,a)}

¹*Beijing Key Laboratory for Magneto-Photoelectrical Composite and Interface Science, School of Mathematics and Physics, University of Science and Technology Beijing, Beijing 100083, People's Republic of China*

²*State Key Laboratory of New Ceramics and Fine Processing, School of Materials Science and Engineering, Tsinghua University, Beijing 100084, People's Republic of China*

(Received 1 October 2016; accepted 2 January 2017; published online 19 January 2017)

Substrate has great influences on materials syntheses, properties, and applications. The influences are particularly crucial for atomically thin 2-dimensional (2D) semiconductors. Their thicknesses are less than 1 nm; however, the lateral sizes can reach up to several inches or more. Therefore, these materials must be placed onto a variety of substrates before subsequent post-processing techniques for final electronic or optoelectronic devices. Recent studies reveal that substrates have been employed as ways to modulate the optical, electrical, mechanical, and chemical properties of 2D semiconductors. In this review, we summarize recent progress upon the effects of substrates on properties of 2D semiconductors, mostly focused on 2D transition metal dichalcogenides, through viewpoints of both fundamental physics and device applications. First, we discuss various effects of substrates, including interface strain, charge transfer, dielectric screening, and optical interference. Second, we show the modulation of 2D semiconductors by substrate engineering, including novel substrates (patterned substrates, 2D-material substrates, etc.) and active substrates (phase transition materials, ferroelectric materials, flexible substrates, etc.). Last, we present prospectives and challenges in this research field. This review provides a comprehensive understanding of the substrate effects, and may inspire new ideas of novel 2D devices based on substrate engineering.

Published by AIP Publishing. [<http://dx.doi.org/10.1063/1.4974072>]

TABLE OF CONTENTS

I. INTRODUCTION	1
II. EFFECT OF SUBSTRATES ON 2D SEMICONDUCTORS	3
A. Interface strain	4
B. Charge transfer	5
C. Dielectric screening	8
D. Optical interference	9
III. MODULATION OF 2D SEMICONDUCTORS BY SUBSTRATE ENGINEERING	10
A. Alteration, patterning, and modification of substrates	10
B. 2D materials as substrates	12
C. "Active" substrates	14
D. Flexible or stretchable substrates	15
IV. PROSPECTIVES AND CHALLENGES	16

I. INTRODUCTION

Substrate is a solid supporting material upon which as-fabricated products or devices adhere. A substrate can be inorganic or organic, rigid or soft, and conducting, semi-conducting

or insulating. It plays great roles in fields ranging from materials synthesis, micro-/nano-fabrication, to device performance and integration. For example, epitaxial growth of strongly correlated oxides on crystalline substrates has been intensively studied for decades.^{1,2} Substrate-engineered high-mobility field effect transistors (FETs) have also been deeply investigated for various semiconducting channel materials.³ Since nano-materials emerge as the potentially key materials in future electronics, their syntheses, properties, and applications have been hot topics in scientific research for more than two decades.⁴⁻⁸ However, their properties are quite susceptible to supporting substrates due to their ultra-small size in at least one dimension. It thus delivers lots of interesting phenomena because of various types of interactions between nano-materials and substrates, and offers a route to modulate properties of nano-materials by substrate engineering.

Among a variety of nano-materials, two-dimensional (2D) materials have been rising stars in materials science since the discovery of graphene in 2004.⁹ In 2D materials, electrons and phonons are limited in the planar dimension, leading to numerous unique properties that deviate from their bulk counterparts.⁹⁻¹¹ A good example is graphene, which has massless Dirac fermions¹¹ and possesses ultrahigh electrical mobility,⁹ excellent thermal conductivity,¹² as well as extremely high strength and modulus.¹³ However, its intrinsic zero bandgap

^{a)}Author to whom correspondence should be addressed. Electronic mail: liuk@tsinghua.edu.cn

limits its wide applications in semiconductor industries. Opening of its bandgap requires complex techniques (for example, defining nanoribbons)¹⁴ and thereby raises the cost of production. Consequently, 2D semiconductors have aroused growing interests in recent years. Typical 2D semiconductors include transition metal dichalcogenides (TMDs),^{15,16} black phosphorous,¹⁷ MXenes,¹⁸ graphdiyne,¹⁹ etc., among which 2D semiconducting TMDs have been intensively investigated owing to their diversity in band structures,²⁰ facile fabrication of heterostructures,²¹ and great potential for electronic device applications.^{22–24} Monolayer semiconducting TMDs, such as MoS₂, WS₂, MoSe₂, and WSe₂ (Fig. 1(a)), have direct bandgaps, in contrast to indirect bandgaps in their bulk counterparts (Fig. 1(b)).^{15,16} Their photoluminescence (PL) efficiency is thus dramatically enhanced at the monolayer limit (Fig. 1(c)) and their bandgap increases with decreasing the number of layers (Figs. 1(b) and 1(d)), potentially inspiring novel optoelectronic applications.^{25–28} Because of the dimensional limitation and the heavier effective mass of carriers, the binding energy of excitons in TMDs is one order of magnitude higher than that in traditional semiconductors,^{29,30} which greatly affects the efficiency of optoelectronic devices, including photodetectors, solar cells, and light emitted diodes. The exciton lifetime is even longer in heterostructures constructed with 2D semiconductors like MoSe₂/WSe₂.³¹ On the other hand, the carriers in the TMDs are with valley index. This intrinsic freedom of electrons can be exploited to develop novel spintronic and valleytronic devices.^{32–34} Recently, defects or edges in WSe₂ are employed as sources of single photon emission owing to spatially localized excitons, finding potential applications in the quantum information processing.^{35–38}

Modulation of properties of 2D semiconductors is of vital importance for their ultimate applications. Their ultra-thin nature has them susceptible to ambient conditions and modulated by various approaches. Electrostatic gating,^{39,40} chemical doping,^{41–43} and strain^{44–46} have been utilized to

modulate both optical emission and electrical conductivity of 2D semiconductors. Substrate effects are also important factors. The roughness, dielectric constant, charge impurity, and defects in a substrate would distinctly affect the properties of 2D semiconductors. Such substrate effects can be exemplified by the difference in PL between suspended and supported 2D semiconductors. Figure 2(a) shows an optical image of mono- and few-layer MoS₂ mechanically exfoliated on a Si/SiO₂ wafer with etched holes. The PL intensity of the monolayer MoS₂ is much enhanced in the suspended regions compared with the supported regions (Fig. 2(b)), suggesting a higher quantum yield of PL for suspended monolayer MoS₂.¹⁵ In chemical-vapor-deposited (CVD) monolayer MoS₂ (Fig. 2(c)), similar result is also observed (Fig. 2(d)).⁴⁷ Besides the different quantum yields, PL peak energy of suspended monolayer MoS₂ is different from that of supported samples as well. As shown in Fig. 2(e), a suspended monolayer MoS₂ shows a strong PL peak at 1.90 eV,¹⁵ in sharp contrast to the much weaker PL centered at 1.83 eV.^{16,48} This great divergence in the transition energy and the quantum yield of PL emission mostly results from the effect of substrates. In the suspended regions, MoS₂ is neutral or less doped, and the emission from the exciton with a high quantum yield is dominant. On a Si/SiO₂ substrate, however, MoS₂ is negatively charged by the substrate, forming trions in MoS₂, and the PL emission thus primarily comes from trions with a low quantum yield and a red-shifted peak (Fig. 2(e)).⁴⁸

In addition to the shift and the enhancement of PL, suspended MoS₂ exhibits enhanced electrical properties compared with MoS₂ supported on a substrate. The performance of supported and suspended MoS₂ FETs and phototransistors were compared in literature,^{47,48} also shown in Figs. 2(f) and 2(g). Here, the supported device was prepared on an n-doped silicon substrate covered with a 300 nm-thick SiO₂ layer, and the suspended one was achieved by under-etching the SiO₂

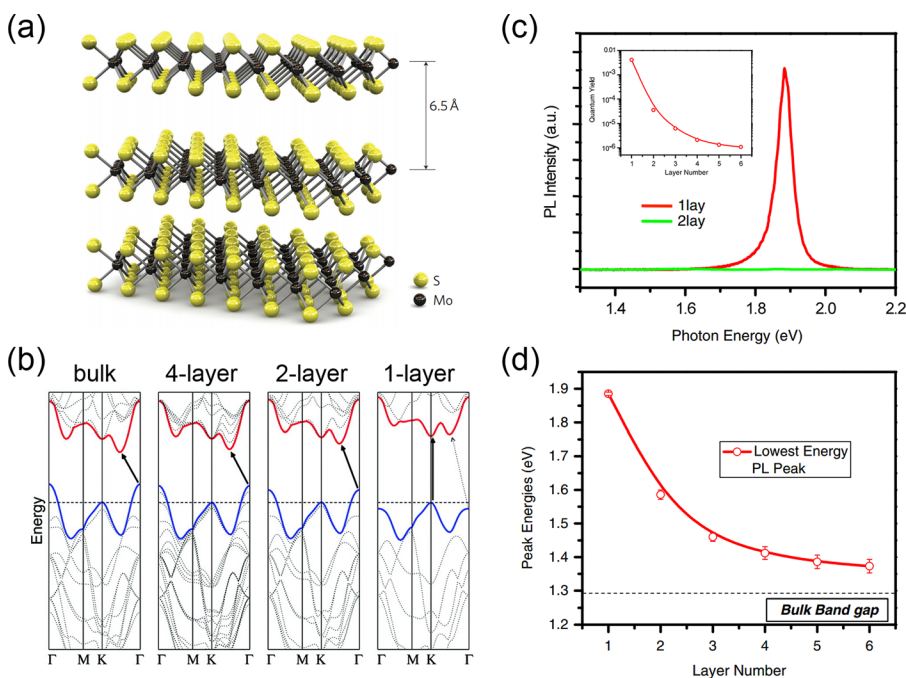


FIG. 1. (a) Schematic of the atomic structure of a typical layered 2D TMDs, MoS₂.²² (b) Calculated band structures of bulk, quadrilayer, bilayer, and monolayer MoS₂, by density functional theory.¹⁶ (c) PL spectra for suspended monolayer and bilayer MoS₂ under an excitation at 2.33 eV.¹⁵ (d) Band-gap energy of thin layers of MoS₂, obtained from the lowest energy peak in PL spectra.¹⁵ Reprinted with permission from Radisavljevic *et al.*, Nat. Nanotechnol. **6**, 147 (2011). Copyright 2011 Macmillan Publishers Limited; Splendiani *et al.*, Nano Lett. **10**, 1271 (2010). Copyright 2010 American Chemical Society; Mak *et al.*, Phys. Rev. Lett. **105**, 136805 (2010). Copyright 2010 The American Physical Society.

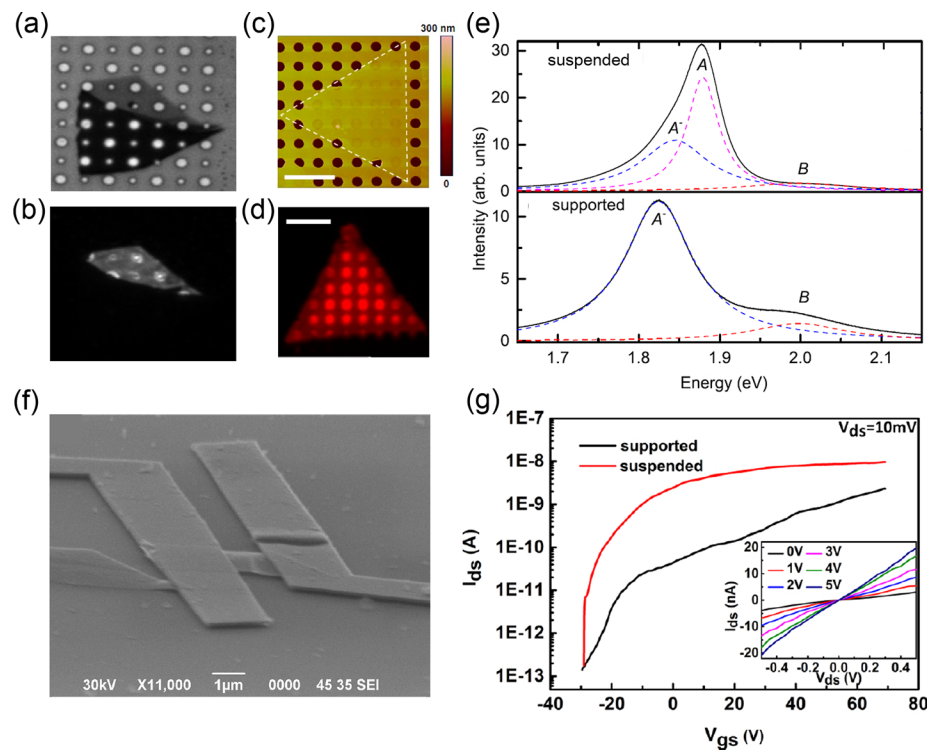


FIG. 2. Photoluminescence and electrical transport measurements of suspended and supported monolayer MoS₂. (a) Optical image of mono- and few layer MoS₂ on a Si/SiO₂ substrate with etched holes 1.0 μm and 1.5 μm in diameter.¹⁵ (b) Mapping of PL peak intensity in the same region.¹⁵ (c) AFM topography of a triangle, synthesized monolayer MoS₂ transferred onto a holey Si/SiO₂ substrate.⁴⁷ (d) Mapping of PL peak intensity from a triangle monolayer sitting on the holey substrate.⁴⁷ (e) PL spectra of suspended and supported monolayer MoS₂ on a Si/SiO₂ substrate (solid lines). Dotted lines show fit functions of A, B, and A⁻ peaks.⁴⁸ The monolayer MoS₂ on Si/SiO₂ substrates is effectively n-type doped by the substrate. The PL peak at \sim 1.83 eV originated primarily from the A⁻ peak (trion) and not from the exciton (A). (f) SEM image of a suspended MoS₂ device. (g) Transfer curves of suspended and supported devices. Inset shows I-V curves at various gate voltages. Note that I_{ds} is the source-drain current, V_{gs} the gate-source voltage, and V_{ds} the applied source-drain voltage.⁴⁹ Reprinted with permission from Mak *et al.*, Phys. Rev. Lett. **105**, 136805 (2010). Copyright 2010 The American Physical Society; Liu *et al.*, Nano Lett. **14**, 5097 (2014). Copyright 2014 American Chemical Society; Scheuschner *et al.*, Phys. Rev. B **89**, 125406 (2014). Copyright 2014 American Physical Society; Jin *et al.*, J. Appl. Phys. **114**, 164509 (2013). Copyright 2013 AIP Publishing LLC.

layer (Fig. 2(f)). The carrier mobility of the suspended device is higher than the value of its supported counterpart by two to tenfold,⁴⁹ leading to a much enhanced electrical conductivity (Fig. 2(g)). This difference results from the interactions between 2D semiconductors and substrates, where defects or impurities at the interface are known to affect the electronic structure⁵⁰ and the performance of devices.^{51,52} Due to the interactions, band structure distortions were observed in supported devices as well.⁵³

The substrate effects also depend on the type of substrates. For instance, monolayer MoS₂ on hexagonal boron nitride (h-BN) flakes is found to have a much stronger PL emission than that on Si/SiO₂ substrates.⁵⁴ Recently, detailed studies of PL emission from thin MoS₂ supported on or capped with different insulating materials reveal the importance of the interaction between MoS₂ and its dielectric surroundings.^{55,56} These results not only suggest the significant effect of substrates on the properties of 2D semiconductors but also reveal the great role of substrates in the performance of 2D devices.

In this review, we summarize recent studies upon the effects of substrates on 2D semiconductors, through viewpoints of both fundamental physics and device applications. We focus our discussions on 2D TMDs because this type of 2D semiconductors is the most important group of 2D

semiconductors that has been intensively investigated. First, we discuss various effects of substrates on the properties of 2D semiconductors, including interface strain, charge transfer, dielectric screening, and optical interference. Second, we show the modulation of 2D semiconductors by substrate engineering, including novel substrates (patterned substrates, 2D-material substrates, etc.) and active substrates (phase transition materials, ferroelectric materials, flexible substrates, etc.). Last, we present prospectives and challenges in this research field. This review provides a comprehensive understanding of the substrate effects and may inspire new ideas of novel 2D devices based on substrate engineering.

II. EFFECT OF SUBSTRATES ON 2D SEMICONDUCTORS

As we described in the Introduction, the PL peak position and PL intensity of a monolayer TMDs is strongly dependent on the substrate where it sits. The mechanism behind this, however, is rather complicated. In 2D semiconductors such as MoS₂ monolayers, recombination of excitons (electron-hole pairs) or trions (electron-electron-hole clusters), depending on the background free electron density, dominates the PL spectrum.^{30,39} Charge transfer between the monolayer and substrate can alter the free carrier density of

the monolayer, and then affect the spectral weights of excitons and trions.^{54,56,57} Dielectric screening of Coulomb potentials is also found to affect the binding energies of excitons and trions, hence their PL intensities.⁵⁸ Strain, which may be imposed to the monolayer by the substrate, is another factor to affect the PL of the monolayer.^{44,59} Last, optical interference, resulting from multi-reflection and multi-refraction at the interfaces, can enhance or weaken the local electric fields (E-fields) around the monolayer, which also affects PL and Raman peak intensity.^{54,60,61}

The entangled and complicated mechanisms of substrate effect, to some extent, are contributed to multiple functions of a substrate. For example, commonly used Si/SiO₂ substrate actually contains many factors affecting a 2D TMD overlayer. First, the surface roughness may change the mechanical coupling and charge transfer efficiency between 2D TMDs and the substrate.⁵⁶ Second, the SiO₂ dielectric layer functions as a cavity for optical interferences, leading to strengthened or weakened incident and emission E-field of light dependent on the thickness of SiO₂. Third, the Si/SiO₂ substrate contains defects and impurities, which may harbor many atmospheric gases, chemical adsorbates, unknown functional groups, and impurity charges.⁴⁹ All these adsorbates could dope 2D TMDs, alter their carrier densities, and lower their carrier mobilities due to interface scattering. Layered materials with atomic flatness, such as h-BN, have few dangling bonds and functional groups, and thus, they can be alternative substrates in devices based on 2D TMDs. Researchers often exploited different types of substrates to clarify substrate effects and underlying mechanisms. In the following, we will discuss various mechanisms of substrate effects.

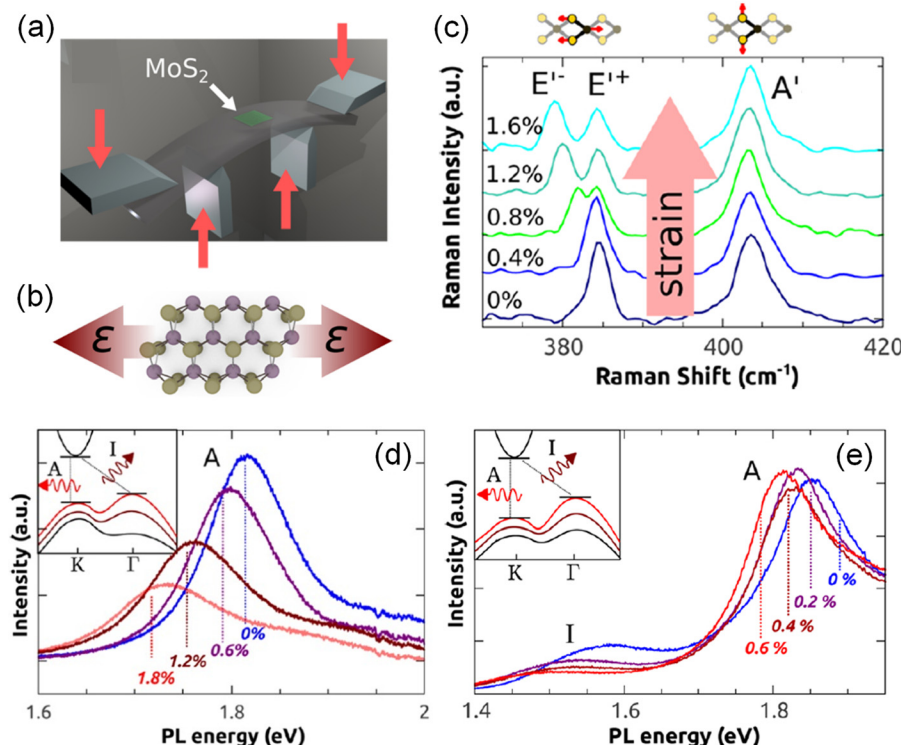
A. Interface strain

Strain is an important factor in determining physical properties of 2D semiconductors for high-performance devices, especially for flexible and stretchable devices.^{62–64} Mechanical bending or stretching of a substrate is typically used to control the strain in 2D materials. In-plane mechanical strain has been shown to strongly modify electronic band structures of 2D semiconductors. In exfoliated monolayer MoS₂, for example, there exists a direct-to-indirect transition of the optical bandgap under a tensile strain exceeding 1%, which leads to a red shift of PL peak and a reduction of PL intensity.^{44,65–67} Moreover, strain directly modifies phonon modes in 2D materials:^{44,59} a uniaxial tensile strain can readily soften the in-plane phonon vibration.^{44,59,68,69} The frequency of in-plane E_{2g}^1 Raman mode is known sensitive to strain, which red-shifts as the strain increases, while the frequency of out-of-plane A_{1g} Raman mode is nearly unchanged under different strains. This phenomenon is observed in both monolayer and few-layer MoS₂.^{44,46,59,68,69}

There are several possibilities to induce strain in overlayer 2D semiconductors by substrates. 2D semiconductors are usually monolayer, ultrathin, and relatively huge in area, and they are coupled to substrates through weak van der Waals interactions. The van der Waals forces may become high enough to deform ultrathin 2D semiconductors

as they are proportional to the contact area between 2D semiconductors and substrates. Whether such a deformation occurs strongly depends on the mechanical property, the thickness, and the initial state of 2D materials, as well as the stress transfer efficiency between 2D materials and substrates. In exfoliated samples, strained wrinkles or ripples could be created if the exfoliation process is not carried out so uniformly. In as-grown CVD samples, a built-in strain usually exists, which could be ascribed to the mismatch of thermal expansion coefficients between 2D materials and substrates during the cooling process in the CVD growth. The interfacial contamination on the growth substrate resulting from the growth process may also contribute to the non-uniform, built-in strain. As a result, the PL intensity and the A exciton peak position of as-grown samples will be changed.^{70,71} This built-in strain may be partially or fully released after a transfer of as-grown 2D materials to another substrate, which is verified by the fact that the field-effect mobility of transferred monolayer MoS₂ is comparable or superior to that of mechanically exfoliated MoS₂.⁷¹ Other ways to apply mechanical strain include engineering of 2D materials by an elastic polymer substrate^{44,45,59,68–70,72} and deposition of metal nanoparticles on 2D materials,^{46,73} where changes in PL and Raman spectra can be observed.

On polymer substrates, polymer caps or metal clamps are applied on 2D materials to avoid sample slippage and enable an effective stress transfer between 2D materials and substrates.^{44,45,68,69} If no clamps used, slippage could occur and only partial strain was transferred from the polymer substrate to the overlayer 2D flakes.⁷⁰ Figure 3 shows a typical evolution of Raman and PL spectra of monolayer and bilayer MoS₂ under strain. To quantify the applied strain, MoS₂ is clamped by metal pads on a polycarbonate (PC) beam that is controllably bent in a four-point bending apparatus (Fig. 3(a)). Therefore, uniaxial strain is applied to MoS₂ lattice, as illustrated in Fig. 3(b). In the unstrained monolayer, in-plane E_{2g}^1 mode at 384 cm⁻¹ and out-of-plane A_{1g} mode at 403 cm⁻¹ can be observed (navy blue line in Fig. 3(c)). The interval between the two modes has been used as an indicator of the layer number of an ultrathin exfoliated MoS₂ flake.^{74,75} When a uniaxial strain is applied on a monolayer MoS₂ by bending the substrate (Fig. 3(a)), the out-of-plane mode (labelled as A' in Fig. 3(c)) shows no measurable shift in position while the degenerate in-plane mode splits into two peaks (labelled as E'^- and E'^+ in Fig. 3(c)) with the increase in the strain. The E'^- peak red-shifts by 4.5 ± 0.3 cm⁻¹/% strain, while E'^+ peak by 1.0 ± 1.0 cm⁻¹/% strain for monolayer. The error of the latter value is almost within the Raman spectral resolution. The redshift of E_{2g}^1 Raman peak is also reported in few-layer MoS₂.⁶⁹ The PL peak in the unstrained monolayer at \sim 1.83 eV is attributed to the recombination of trions at the K point for the direct bandgap transition (Fig. 3(d), inset), because MoS₂ is effectively n-type doped by the substrate. With the increase in strain, this peak red-shifts almost linearly along with a decreased intensity (Fig. 3(d)), indicating a transition from direct to indirect bandgap and a reduction in the bandgap energy (Fig. 3(d), inset).⁴⁴ The PL spectrum of an unstrained bilayer MoS₂ in Fig. 3(e) shows an A exciton peak at \sim 1.81 eV (direct bandgap transition) and an I peak at



~1.53 eV (indirect bandgap transition). Both A and I peaks also red-shift with increasing the strain, but their intensities do not change much.^{44,68} This result indicates that the bilayer MoS₂ are always of indirect bandgap type within the range of the applied uniaxial strain (inset of Fig. 3(e)).

The physical mechanism of the strain effect originates from the renormalization of electronic band structures of 2D semiconductors. According to the theoretical calculations, the bandgap of monolayer 2D semiconductors reduces with the increase in strain, and when the strain reaches a threshold, the monolayer material will transit from a direct bandgap to an indirect bandgap (inset of Fig. 3(d)).^{44,59,65–67,69} This picture can explain the redshift of PL peak and the reduction of PL intensity for monolayer MoS₂. Strain can also affect the electron-phonon interaction. When applied a tensile strain, the in-plane Raman mode can be distinctly affected, while the out-of-plane mode is not obviously changed.

For other 2D semiconductors, however, the strain effect may behave in other ways because of the different evolution of band structures under strain. In a bilayer WSe₂, for example, a distinct enhancement of PL intensity appears under a uniaxial tensile strain, inverse to the previous results in mono- and few-layer MoS₂ as shown in Figs. 3(d) and 3(e). Figure 4(a) reveals the PL evolution of bilayer WSe₂ with strain. An enhancement in PL intensity is clearly shown as strain increases. The PL peak intensity of the unstrained bilayer WSe₂ is drastically less than that of the unstrained monolayer WSe₂, which is also shown in Fig. 4(a) for a reference. As strain increases, the second peak appears at a higher energy, red-shifts, and strengthens significantly in intensity. The PL intensity of the bilayer WSe₂ at a strain ~1.5% is comparable to that of the unstrained monolayer. Based on the results of

FIG. 3. Evolution of Raman and PL spectra of mono- and bilayer MoS₂ under a uniaxial strain. (a) Schematic of the beam bending apparatus used to strain MoS₂. (b) Schematic illustration of the MoS₂ lattice under a uniaxial strain (top-view). (c) Raman spectra of monolayer under strains ranging from 0% to 1.6%. (d) PL spectra of monolayer as strained from 0% to 1.8%. (e) PL spectra of bilayer as strained from 0% to 0.6%. Insets in (d) and (e) show schematic illustrations of the band structures for mono- and bilayer MoS₂ that are strained from 0% (black) to ~5% (maroon) and ~8% (red). Reprinted with permission from Conley *et al.*, Nano Lett. **13**, 3626 (2013). Copyright 2013 American Chemical Society.

density functional theory (DFT) calculations, the distinct PL enhancement and reduction of full width at half maximum (FWHM) is attributed to an indirect to direct bandgap transition for the strained bilayer WSe₂. Figure 4(b) compares the calculated electronic band structures for bilayer WSe₂ at 0% and 1.5% tensile strain. In contrast to bilayer MoS₂, the energy difference between the direct and indirect bandgaps of unstrained bilayer WSe₂ is much smaller, only ~40 meV. The 1.5% strain changes the conduction band (CB) minima, with the direct CB valleys K_C moving down by 86 meV while the indirect CB valleys Σ_C moving up by 27 meV in energy. Thus, a crossover from indirect to direct bandgap should occur in bilayer WSe₂. This picture could explain the increase in PL intensity in Fig. 4(a).⁴⁵ In monolayer WSe₂, which is of intrinsically direct bandgap, PL intensity also shows a drastic increase with strain (Fig. 4(c)). It originates from the fact that as strain increases, monolayer WSe₂ remains more like a direct bandgap semiconductor because its direct bandgap becomes much less than indirect bandgap, which is different from the behavior of monolayer MoS₂ that undergoes a direct to indirect bandgap transition in the same case.

B. Charge transfer

In semiconductor devices, work function (WF) or Fermi level is a primary parameter determining the direction and efficiency of charge transfer in metal-semiconductor contact and p-n junction. Electrons move from a material with a pristinely higher Fermi level to that with a lower one unless the diffusion electron flux balances with the drift electron flux. In this process of charge transfer, the accumulation of surface charges in semiconductors causes a surface potential, which is simply equal to the difference of work functions

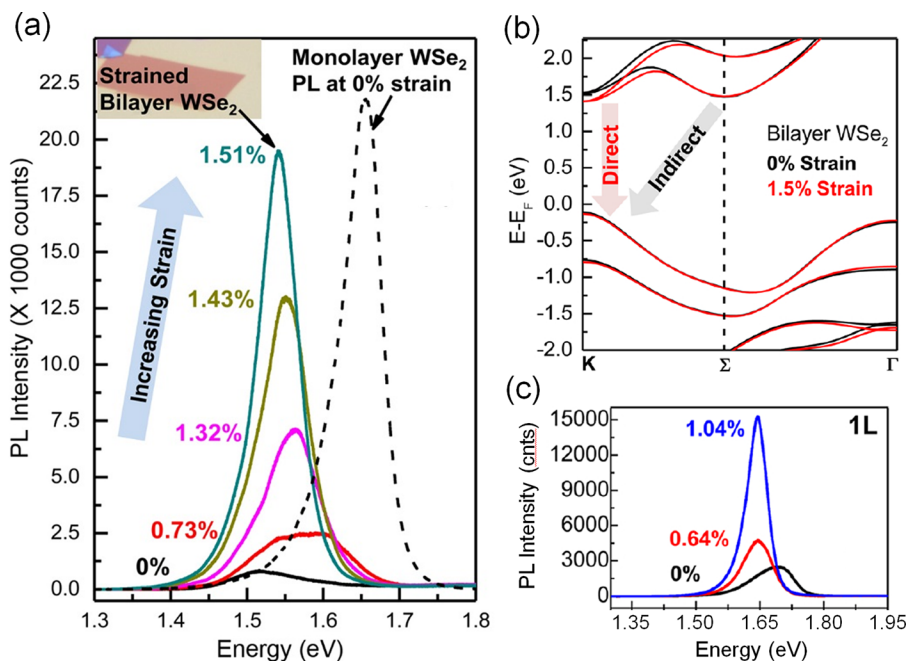


FIG. 4. (a) PL spectra of bilayer WSe₂ at different strain. PL of unstrained monolayer WSe₂ is shown for comparison. Inset: optical image of the bilayer WSe₂ used. (b) Electronic band structure for bilayer WSe₂ with and without strain based on the DFT calculation. CB and VB changes under strain are clearly seen with the K point CB minima decreasing distinctly whereas the Σ point CB minima increase slightly, thus showing an indirect to direct bandgap transition. (c) PL spectra of monolayer WSe₂ at different strain. Reprinted with permission from Desai *et al.*, Nano Lett. **14**, 4592 (2014). Copyright 2014 American Chemical Society.

divided by an electron charge. Surface potential and work function can be influenced by surface states. For example, substrate-induced charge traps can significantly alter the surface potential and work function of 2D semiconductors such as MoS₂. Scanning Kelvin probe microscopy measurements show that surface potential of MoS₂ will decrease due to the enhanced charge transfer in a supported monolayer on SiO₂/Si substrate, compared with a suspended one, because MoS₂ is probably n-type doped by the substrate.^{76,77} In other words, the charge transfer between TMDs and substrates can modulate the electronic structure of 2D TMDs, which greatly impacts carrier transport behaviors and optical properties, including PL, Raman, and reflectance contrast spectra. On the other hand, charge transfer may co-exist with other charge-related effects, such as dielectric screening which we will discuss in Sec. II C, to influence the material properties in different ways. It means that in many cases, the observed changes in physical properties of 2D materials are not necessarily only related to charge transfer or only dielectric screening.

A substrate may harbor many kinds of atmospheric gases, chemical adsorbates, unknown functional groups, and impurity charges.⁴⁹ Such adsorbates, as well as defects in substrates, may function as charge traps to dope 2D semiconductors, affecting its surface potential and charge distribution by charge transfer. For example, due to the polarity and hydrophilicity of MoS₂ and WS₂, substrate-borne water moisture would strongly affect their properties. A trace amount of moisture at the interface may substantially lower the PL efficiency of MoS₂ and WS₂ monolayers by n-type doping. The resulting weaker, broader, and red-shifted PL can be found at the monolayers transferred onto many of dielectric substrates, including Si/SiO₂, ITO glass, quartz, LaAlO₃, and SrTiO₃. The n-type doping effect is further verified by the red-shift of the A_{1g} peak that indicates the concentration of electrons.⁵⁵ These phenomena are very similar

to the doping results from molecular dopants.^{41,78} When a monolayer 2D semiconductor is located on a metallic substrate (e.g., Au) or a few-layer graphene (FLG), it could be also doped by direct charge transfers.⁵⁴

The substrate-induced charge transfer exerts a strong influence on the PL property of monolayer MoS₂. The charge transfer between the substrate and monolayer MoS₂ modifies the excitonic states, resulting in a switch between the emissions from neutral excitons and from charged excitons (trions) in MoS₂. The injected or depleted electrons in MoS₂ change the Fermi energy E_f and as a result tune the concentration ratio of neutral to charged excitons.^{54,56,57} Due to the larger binding energy of charged excitons, recombination of charged excitons emits light at a lower energy than that of neutral excitons, inducing a PL emission at a longer wavelength from charged excitons. The lower quantum yield of emission from charged excitons also leads to a weaker PL intensity, compared to the emission from neutral excitons. The substrate-induced effect of charge transfer on both PL peak position and PL intensity for monolayer MoS₂ is observed in experiments. Figure 5(a) shows PL spectra of monolayer MoS₂ on different substrates. The A and B excitons peak at \sim 655 nm and \sim 630 nm, respectively. Another peak at \sim 670 nm is associated with the emission from charged A exciton (A⁻). Both the wavelength and the intensity of PL emission are dependent on substrates. The spectral weight ratio of neutral to charged excitons in the PL spectra are also modified by substrates, which is related to the doping level of MoS₂.⁵⁴ The PL peak wavelength for monolayer MoS₂ shows a large blue-shift (\geq 10 nm) on Au, Gel-Film[®], few-layer graphene (FLG), and h-BN, compared to that on SiO₂ and mica. This blue-shift can be explained by the increased contribution in PL from neutral excitons. On SiO₂, however, many reports have indicated the n-type doping of MoS₂ by the substrate, and thereby, the PL is dominated by charged excitons.^{28,39,48,57}

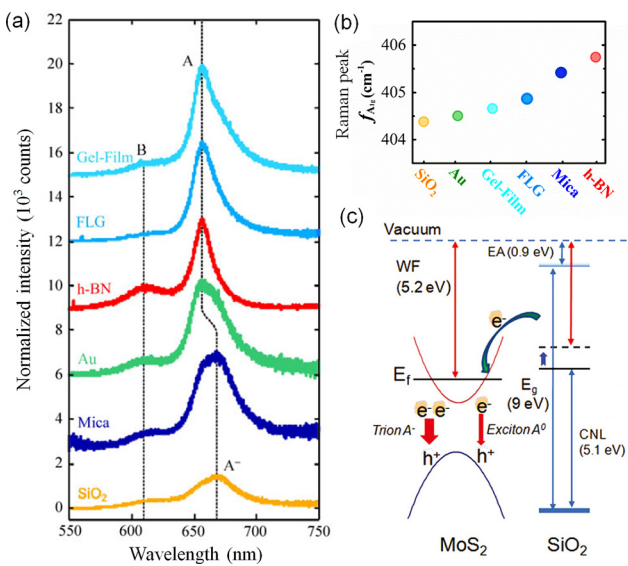


FIG. 5. (a) PL spectra of monolayer MoS₂ on Gel-Film, FLG, h-BN, Au, mica, and SiO₂. Spectra are corrected for interference effects and are shifted vertically for clarity. The dashed black lines indicate the positions of peak emission, including the A (neutral), A⁻ (charged) and B exciton transitions.⁵⁴ (b) Frequencies of the Raman A_{1g} mode as a function of substrate material.⁵⁴ (c) Schematic diagram of energy level and doping effect between monolayer MoS₂ and SiO₂.⁵⁷ Reprinted with permission from Buscema *et al.*, *Nano Res.* **7**, 561 (2014). Copyright 2014 Tsinghua University Press and Springer-Verlag Berlin Heidelberg; Li *et al.*, *Nanoscale* **6**, 15248 (2014). Copyright 2014 The Royal Society of Chemistry.

As we discussed in Sec. II A, the Raman active E_{2g}^1 mode is sensitive to the in-plane strain in the monolayer of 2D TMDs, while the A_{1g} mode is barely affected by the strain. However, when the charge transfer dominates the interactions between TMD layers and substrates, it shows a softening and broadening of the A_{1g} phonon with electron doping, whereas E_{2g}^1 mode remains essentially inert.⁷⁷ Raman spectra of monolayer MoS₂ deposited on different substrates show that the position of E_{2g}^1 peak is insensitive to the substrate material, with a deviation of less than ~ 0.4 cm⁻¹. But the frequencies of A_{1g} mode are shifted by ~ 2 cm⁻¹ as shown in Fig. 5(b). It can be ascribed to two factors: the doping from substrates that affects the electron density in MoS₂ and the change in the strength of dipolar interactions between MoS₂ layer and different substrates.⁵⁴ Figure 5(c) shows the schematic energy band diagram of the interfacial charge transfer for monolayer MoS₂ on SiO₂ substrate. The work function (WF) of MoS₂ used here is 5.2 eV. The electron affinity (EA), band gap (E_g), and charge neutral level (CNL) of SiO₂ is shown in Fig. 5(c). The substrate with the larger energy difference between the CNL and WF of MoS₂ is assumed to inject more electrons into MoS₂, causing a stronger doping effect, and in turn the PL spectra exhibits a higher relative intensity ratio of charged to neutral excitons. The defects located at interface form trap states and redefine the CNL (dashed line in Fig. 5(c)), and n-doping effects were observed as reported.⁵⁷

Substrate-doping effect on CVD monolayers of MoS₂, WS₂, and WSe₂ has also been reported by Yu *et al.*⁵⁵ PL and Raman spectra of monolayer MoS₂ grown by CVD and

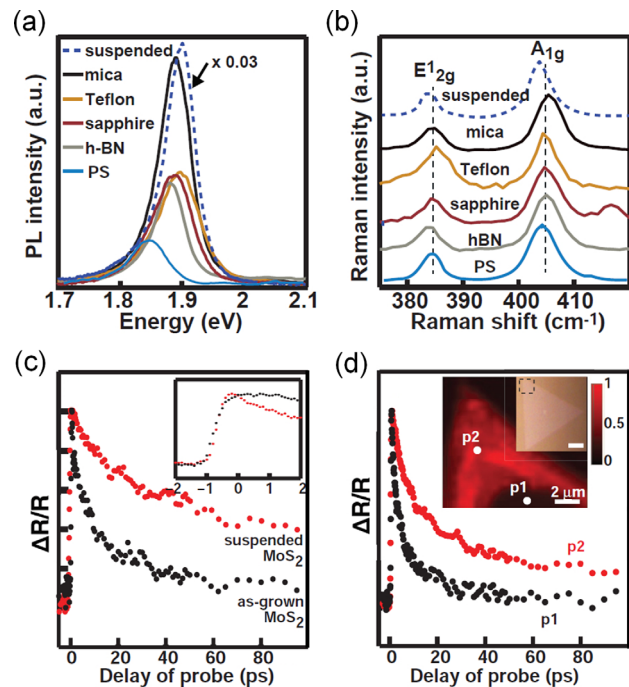


FIG. 6. (a) PL spectra of as-grown monolayer MoS₂ on sapphire substrates (red) and the monolayer transferred onto mica (black), h-BN (gray), and Teflon (orange), and polystyrene (blue) substrates. PL of suspended monolayer MoS₂ with the intensity scaled by a factor of 0.03 is also given. The PL of the monolayers on Teflon substrates is scaled down by a factor of 1.6 due to the local field enhancement caused by the low refractive index of the substrate. (b) Raman spectra of monolayer MoS₂ on different substrates. The two dashed lines indicate the E_{2g}^1 and A_{1g} peaks of the as-grown monolayer. (c) Transient differential reflection collected from suspended and as-grown monolayer MoS₂ on sapphire substrates. (d) Transient differential reflection collected from two different areas on one single flake of WS₂. The p1 is from the central area with low PL, while the p2 from the edge area with high PL as indicated in the PL mapping. Inset: PL mapping and optical image of the flake in which the dashed square indicates where the mapping PL was collected from (scale bar, 10 μ m). Reprinted with permission from Yu *et al.*, *Adv. Funct. Mater.* **26**, 4733 (2016). Copyright 2016 Wiley-VCH Verlag GmbH & Co. KGaA, Weinheim.

transferred on different substrates are shown in Figs. 6(a) and 6(b). According to their observation, mica enables the strongest PL among all substrates, around 2–3 times higher than sapphire. h-BN is not as good as mica in terms of promoting MoS₂ PL. Because the frequency of E_{2g}^1 peak shows little change, strain effect could be excluded (Fig. 6(b)). The higher PL efficiency (intensity) of the supported monolayer is accompanied with a blue-shift of the Raman peak, which indicates a decrease in the n-doping level. The different ratios of trion/exciton emission extracted from the PL spectra show that the higher PL efficiency comes with a lower ratio of trion emission. This is consistent with the results in literature.^{48,54,56,57} Similar effect of substrate-induced doping can be found in monolayer WS₂, where the substrate, such as mica, can mostly promote the PL because of the capability of the substrate to attract electrons (p-doping) from the monolayer. However, the PL of monolayer WSe₂ can be enhanced by an n-doping substrate such as polystyrene and h-BN, but weakened on p-doping substrates. This results from the different intrinsic doping of different types of 2D monolayers, as CVD grown WS₂ and MoS₂ are known

intrinsically n-doped while WSe₂ p-doped. It reveals that even on the same substrate, the substrate-induced doping may cause different effects on the PL efficiency of different 2D monolayers.

Besides the population change of trions/excitons through the charge transfer between 2D monolayers and substrates, substrates also affect the dynamic process of exciton recombination. Yu *et al.* found that the substrate can shorten the exciton lifetime of 2D overlayers. Fig. 6(c) shows the exciton dynamics of suspended and as-grown (on sapphire) monolayers, indicated by the differential reflection $\Delta R/R$ of a delayed probe beam from the monolayer after an excitation of a pump beam. Upon photoexcitation, $\Delta R/R$ arises to its maximum value within ≈ 500 fs for all the monolayers, consistent with the values reported previously.^{77,79} The decay of the charge carriers in the suspended monolayers is obviously slower than that in the supported monolayers. According to the definition of inner quantum efficiency, the slower decay of charge carriers means a longer exciton lifetime and thereby results in a higher PL efficiency. Yu *et al.* observed that the PL at the edge is stronger than that in the center area of as-grown WS₂ monolayers (Fig. 6(d)). The lower PL is often accompanied with a shorter exciton lifetime, suggesting a faster defect-assisted exciton recombination. The defect-assisted nonradiative recombination in the supported monolayers depends on the interaction of the defects in the monolayer with the substrate.⁵⁵ There are other recent literatures claiming that the defect-assisted recombination is the dominant mechanism for nonradiative electron-hole recombination in which the electrons and holes are captured by defects via Auger processes.⁷⁹

Last, it is worth noting that the interface coupling can modulate the efficiency of charge transfer. For example, surface roughness affects the contact and the coupling between 2D semiconductors and substrates, and as such may cause a local variance in the mechanical and electrical properties of 2D layers.^{56,80,81} It is reported that the roughness could result in an inefficient charge transfer and thereby affect the PL lineshapes.⁵⁶

C. Dielectric screening

It is well known that the strong electron-electron or electron-hole Coulomb interactions lead to many-body effects, which play important roles in electrical transports and optical transitions of semiconductors. Coulomb interactions are strongly coupled with dielectric properties of surrounding materials, also known as dielectric screening effect.⁵⁸ The dielectric mismatch between a nanoscale semiconducting material and surrounding environment can result in a number of peculiarities that are not present in bulk.⁸² For example, the dielectric environment can change the exciton binding energy in semiconducting films or nanowires by screening Coulomb interactions and modifying electron-electron interactions.^{83–85} It thus has a crucial influence on optical bandgaps of semiconductors and can strongly modulate both electrical and optical properties of low dimensional materials, including quantum wells,⁸⁶ carbon nanotubes,^{87,88} and graphene.^{89,90}

Based on a picture of fundamental physics, the Coulomb interaction between an electron and a hole in a semiconductor can be screened by the environmental dielectric if the relative dielectric constant of the semiconductor mismatches that of the environmental dielectric, as schematically shown in Fig. 7(a). The screening is reduced if $\epsilon_e < \epsilon_s$, and enhanced if $\epsilon_e > \epsilon_s$, where ϵ_e and ϵ_s are, respectively, dielectric constants of the environment and the semiconductor.⁸² In atomically thin 2D TMDs, the combined effects of reduced dimensionality, relatively large effective mass, and weak effective dielectric screening modify the functional form of the Coulomb interaction, and derives a large exciton binding energy.⁹¹ On the other hand, because the carrier mobility in 2D TMDs is determined by both Coulomb potential scattering and phonon scattering (including intrinsic and extrinsic phonon), it is also relevant to the distribution of Coulomb potential. As shown in Fig. 7(b), the Coulomb potential distribution for two positive and negative point charges becomes more localized with increasing the relative dielectric constants of the environment.⁵⁸ The net potential of the image charges strengthens the total potential if the environmental dielectric constants κ_1 and κ_2 are smaller than the MoS₂ dielectric constant κ_s (upper panel), and diminishes the total potential if κ_1 and κ_2 are larger (lower panels). It indicates that the Coulomb potential scattering of carriers will be reduced with the increase in the relative dielectric constants. Based on the above analysis, it is clearly seen that dielectric screening can impact both exciton binding energy and carrier mobility of 2D TMDs.

However, comprehensive studies of the dielectric screening effect of substrates on 2D TMDs are still lacking. This is partially because the screening effect of substrates often co-functions with or hides behind other strong mechanisms, such as charge transfer and strain. Instead, the influence of dielectric environments on exciton behaviors of 2D TMDs was investigated by surrounding monolayer MoS₂ on a substrate with solvents having different relative dielectric constants.⁵⁸ In this study, blue shifts of PL peaks were observed with the increase in dielectric constants of the surrounding solvents. PL peaks were enhanced and narrowed accordingly, indicating an increase in the exciton/trion weight ratio. It was derived by scaling that binding energies of excitons and trions decrease with the increase in the surrounding dielectric constants. This is attributed to the strongly screened Coulomb potential by dielectrics, which reduces the scattering of excitons/trions by charged impurities (CI) at the interface, thus prolonging the lifetime of quasiparticles. Recently, Chernikov *et al.* optically measured the energies of excitonic states in monolayer WS₂. They found that the effective dielectric screening modifies the Coulomb interactions, leading to a nonhydrogenic Rydberg series of excitonic states in monolayer WS₂.⁹¹ Stier *et al.* studied the effect of the surrounding dielectric environment on monolayer WSe₂ through the diamagnetic shift of the optical transition energy of excitons. The increased dielectric screening was found to increase the exciton size and reduce the exciton binding energy.⁹² All of these experimental results show that the dielectric environment around the atomically thin 2D semiconductors would highly influence their excitonic properties.

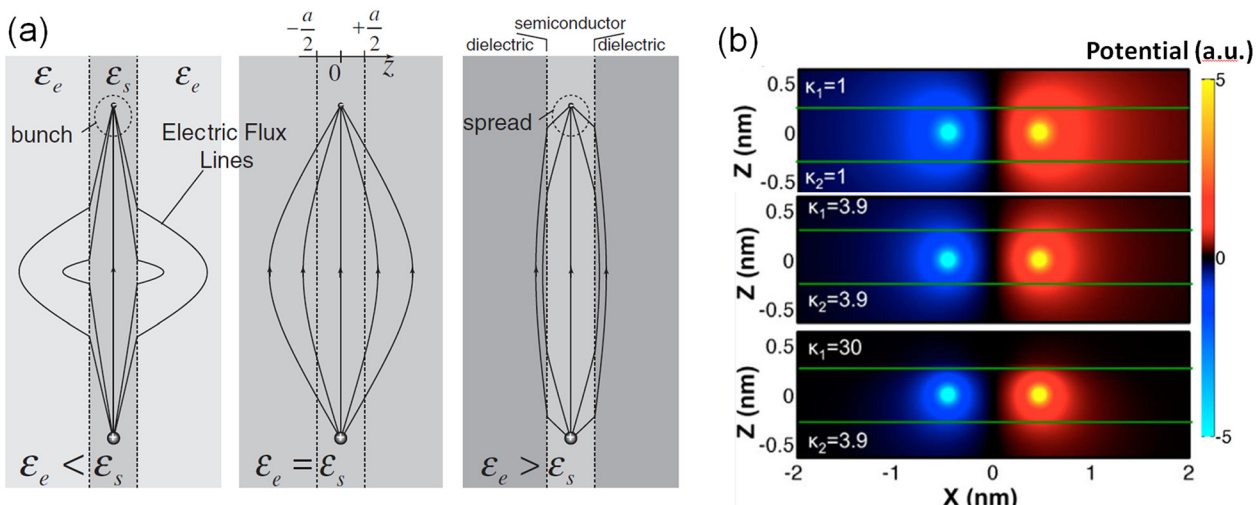


FIG. 7. (a) Electric flux lines from a positive unit charge to an electron considering the effect of the dielectric environment. The flux lines bunch closer inside the semiconductor layer if $\epsilon_e < \epsilon_s$, and spread farther apart if $\epsilon_e > \epsilon_s$, thus enhancing Coulomb interaction in the former case and damping it in the latter.⁸² (b) Coulomb potential distribution with a positive and a negative unit charge in the middle layer of a dielectric-sandwiched structure. The three contours are for different dielectric configurations.⁵⁸ Reprinted with permission from Jena *et al.*, Phys. Rev. Lett. **98**, 136805 (2007). Copyright 2007 The American Physical Society; Lin *et al.*, Nano Lett. **14**, 5569 (2014). Copyright 2014 American Chemical Society.

Carrier mobility is of vital importance on applications of 2D TMDs in electronic and optoelectronic devices. In suspended 2D TMDs, carrier mobility is dominated by scattering from intrinsic acoustic and optical phonons. In supported TMDs, however, it is also limited by scattering from charged impurities, traps, and defects at the semiconductor-dielectric interface, where E-fields could be physically generated by charged impurities⁹³ and dipoles of metal-oxide bonds in dielectric substrates.⁹⁴ The latter case is reported to exist in thiol-treated monolayer MoS₂ supported on different substrates. Figure 8 shows how the carrier transport of monolayer MoS₂ on a substrate is influenced by dielectric screening. The monolayer MoS₂ was mechanically exfoliated on 10 nm high- κ oxide/285 nm SiO₂/Si substrates (Fig. 8(a)). Figure 8(b) shows the field-effect mobility, μ , as a function of temperature for three devices on HfO₂, Al₂O₃, and SiO₂, respectively. It is noticeable that μ increases with increasing the dielectric constant of the oxides. The solid lines in Fig. 8(b) are the best theoretical fits at high temperatures for the three oxide substrates, taking into account intrinsic and substrate surface optical phonons and charged impurities (CIs). Among the three oxide substrates, CI scattering in HfO₂ is the weakest because the Coulomb potential in HfO₂ is mostly screened due to its highest dielectric constant. The effective dielectric screening in a high- κ dielectric substrate originates from the large ionic polarizability of metal-oxide bonds. Figure 8(c) plots the calculated and the experimental room-temperature mobility as a function of CI density, n_{CI} , for the three oxide substrates. Two regimes emerge in the diagram. In the regime of high CI densities, the mobility is limited by CI scattering, and thus, HfO₂ is the best choice among the three oxide substrates due to its strongest dielectric screening. At low CI densities, however, the mobility is limited by phonons and almost independent of n_{CI} . In this regime, HfO₂ is outperformed by the other two oxides, and as a result, relatively low- κ dielectric substrates

such as SiO₂ and boron nitride (BN) would be favorable.⁹⁴ The reduced mobility at low CI densities on HfO₂, compared to that on SiO₂, is also reported by theoretical studies, which is attributed to the higher dielectric constant and softer polar phonon modes.⁹⁵ These results clarify the effect of dielectric screening on the carrier mobility and provide guides for the choice of device substrates.

D. Optical interference

Optical interference, resulting from reflection and refraction at each interface of thin films, can enhance or reduce the local electric fields (E-fields) around the surface depending on optical constants and film thicknesses. It means that the amplitude of local E-fields can be modulated by the optical interference effect. This effect must be considered when a material is ultrathin because in such a case, the properties of the material are very sensitive to the local E-fields around the surface.^{96,97} For example, intensities of Raman signals for graphene strongly depend on both incident local E-field and emitted local E-field.^{60,98,99} This relationship has become the basic concept of designing “hot” spots for surface enhanced Raman signals. In 2D TMDs, intensities of PL signals are also dependent on local E-fields involved in both light absorption (electron excitation from valence to conduction bands) and light emission (the radiative recombination of excitons) processes. Consequently, PL intensities of 2D TMDs can be enhanced or weakened depending on the strengths of local E-fields during the two processes, which is further determined by the thicknesses and the optical constants of substrates when the overlayer material is mono- or few-layer 2D TMDs. When the overlayer 2D TMDs is not so ultrathin, reflection and refraction within the 2D overlayer must also be considered. Note that the interference effect does not perturb the peak emission wavelength but strongly affect the intensity of the emission.^{54,100}

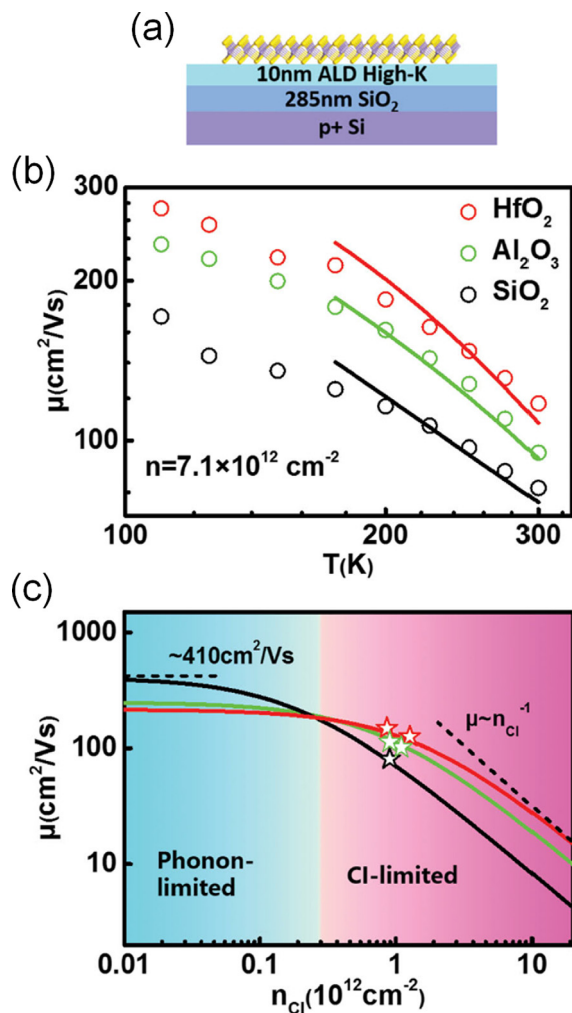


FIG. 8. Effect of dielectric screening on the carrier transport of monolayer MoS₂. (a) Schematic illustration of the device structure. (b) Temperature dependent field-effect mobility for devices on SiO₂ (black), Al₂O₃ (green), and HfO₂ (red), respectively. μ is extracted at $n = 7.1 \times 10^{12} \text{ cm}^{-2}$ for all the three devices. Solid lines are the modeling results at high temperatures. (c) Predicted field-effect mobility as a function of charged impurity density (n_{ci}) for devices on SiO₂ (black line), Al₂O₃ (green line), and HfO₂ (red line) substrate. The symbols are experimentally extrapolated data from five different devices. Reprinted with permission from Yu *et al.*, Adv. Mater. **28**, 547 (2016). Copyright 2015 Wiley-VCH Verlag GmbH & Co. KGaA, Weinheim.

When calculating local E-fields near a 2D overlayer on a substrate, optical paths due to multi-reflection and multi-refraction at each interface must be considered. Li *et al.* proposed a model to calculate the total absorption and emission intensity by considering multiple internal reflections at each interface of the air/MoS₂/SiO₂/Si configuration (Fig. 9(a)) for both the incident and emitted lights.⁶¹ The output Raman intensity from the top MoS₂ layer (total thickness d_1) can be expressed as

$$I = \int_0^{d_1} |A_{ex}(x)A_{sc}(x)|^2 dx,$$

where $A_{ex}(x)$ and $A_{sc}(x)$ are the E-field amplitudes for the excitation and scattering light, respectively. Figure 9(b) shows that the calculation agrees well with experimental

results for the E_{2g}^1 mode in terms of the spectral intensity at various numbers of layers (NL) ranging from 4 to 120 layers. Two maxima of the E_{2g}^1 peak intensity appear at NL ~ 4 and 80. Extending the calculation to a larger NL range reveals the existence of four intensity maxima within 300 layers (inset of Fig. 9(b)), but the corresponding enhancement factors (normalized by the signal from bulk) decay from 10, 3.0, and 1.3 to 1.1, respectively. For NL > 300 , no clear enhancement peaks exist. In addition to the enhancement peaks, valleys due to destructive interference are also observed, which further confirms the interferential nature of the observed spectra. Figure 9(c) shows a contour plot of the enhancement factors (excited at 532 nm) as a function of the NL of MoS₂ and the thickness of SiO₂, d_2 . The irregular traces of enhanced peaks (dotted lines) are characteristics of interference determined by the NL of MoS₂ and d_2 in the interference phase factor $\phi = 2\pi\tilde{n}_1d_1/\lambda_{ex} + 2\pi\tilde{n}_2d_2/\lambda_{ex}$. When the NL of MoS₂ ($\propto d_1$) increases, d_2 has to decrease for maintaining the enhanced condition following $\phi = (N + 1/2)\pi$ (N = integer). This provides a basic reference in optimizing the dielectric thickness for detecting atomic layers. By considering the optical interference, the intensity ratio of the MoS₂ E_{2g}^1 mode to the Raman peak of Si at 520 cm⁻¹ can be used as a rapid criterion for counting the NL of MoS₂, and the most sensitive range spans from 1 to 20 layers, as shown in Fig. 9(d).⁶¹

Zhang *et al.* studied the dependence of Raman and PL intensity of monolayer MoS₂ on the thickness of SiO₂ by using a multi-reflection model based on Fresnel's law.¹⁰⁰ In their study, the monolayer MoS₂ was grown by CVD on SiO₂/Si substrates with different thicknesses of SiO₂. Figure 10(a) shows an optical image of as-grown monolayer MoS₂. Typical PL spectra of monolayer MoS₂ on various SiO₂/Si substrates are shown in Fig. 10(b). The sharp spike observed at ~ 654 nm corresponds to the Si Raman peak, which can be used to normalize the PL spectra. The PL emission from A exciton at ~ 670 nm (~ 1.85 eV) is found to remarkably depend on the SiO₂ thickness. The strongest and the weakest intensities are observed when SiO₂ thicknesses are 328 nm and 192 nm, respectively. Figure 10(c) shows the color contour plot of the enhancement factor for the A exciton emission of monolayer MoS₂, as functions of both SiO₂ thickness and excitation wavelength. Under a fixed excitation wavelength, the PL signals can be enhanced by optimizing the SiO₂ thickness. For example, when a 632.8 nm excitation laser is used, the SiO₂ thickness can be selected to be in the range of 300–350 nm, or 530–570 nm to enhance the A exciton peak in PL.¹⁰⁰

III. MODULATION OF 2D SEMICONDUCTORS BY SUBSTRATE ENGINEERING

A. Alteration, patterning, and modification of substrates

The strong dependence of the performance of 2D semiconductors on a substrate suggests a possibility to modulate their properties by engineering the substrate. Compared with usual modulation approaches such as electrostatic gating and chemical doping, substrate engineering provides an optional

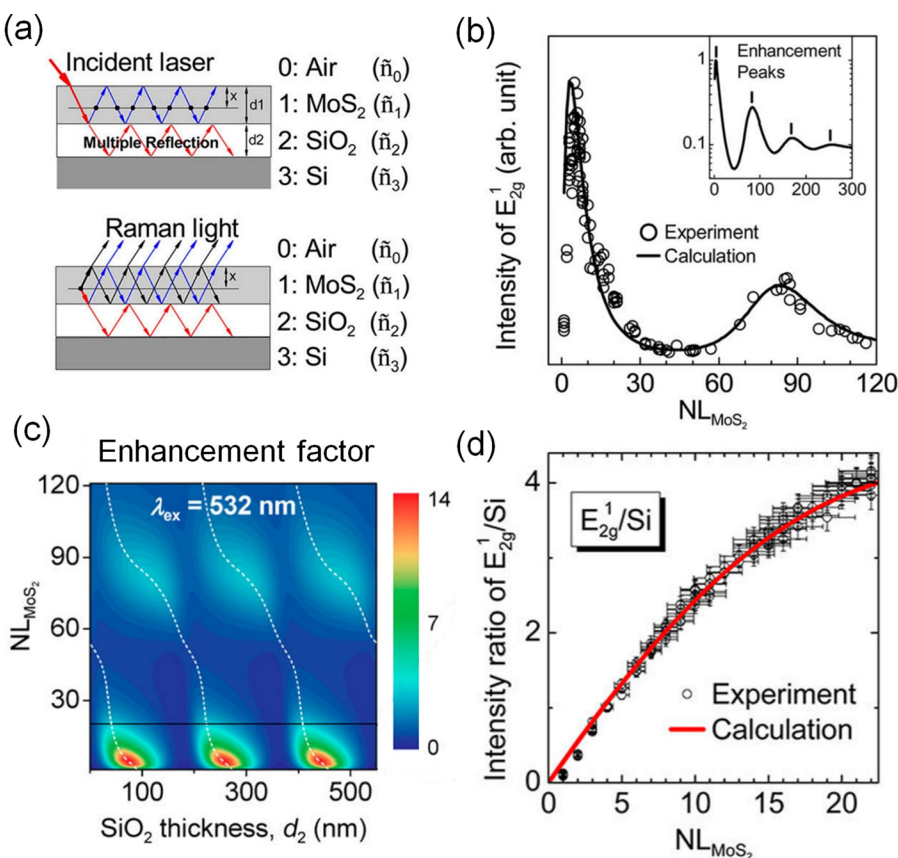


FIG. 9. (a) Schematic diagrams for optical paths of the incident and Raman scattering light, respectively, in the $\text{MoS}_2/\text{SiO}_2/\text{Si}$ configuration. (b) Calculated and experimental E_{2g}^1 peak intensities for MoS_2 with different number of layers (NL). (c) Contour plot of calculated enhancement factors as a function of MoS_2 NL and d_2 at $\lambda_{ex} = 532 \text{ nm}$. (d) Comparison of calculations and experiments for the intensity ratio of the MoS_2 E_{2g}^1 ($\sim 383 \text{ cm}^{-1}$) mode to the Raman peak of Si substrate (520 cm^{-1}). The errors for NL values and intensity ratios are 10% and 5%, respectively. Reprinted with permission from Li *et al.*, ACS Nano **6**, 7381 (2012). Copyright 2012 American Chemical Society.

and facile modulation way without complex chemical processing. Straightforward ideas of substrate engineering include alteration, patterning, or modification of substrates. By altering substrates, Yu *et al.* systematically studied the PL of different types of 2D semiconductors on various substrates (sapphire, Teflon, mica, h-BN, polystyrene, etc.), as described in Section II B.⁵⁵ They found that diverse doping effects, resulting from the substrates and the substrate-borne moisture, strongly modulate the PL efficiency of 2D semiconductors. The defect-assisted nonradiative exciton recombination can suppress the PL efficiency, also deviating the effects of different substrates.

As the second way, patterning of substrates was studied, and attractive results were revealed. For example, Wu *et al.* observed a lasing effect from monolayer WSe₂ introduced as a gain medium at the surface of a pre-fabricated photonic crystal cavity on a gallium phosphide membrane. A continuous-wave nanolaser operating at about 740 nm was obtained with an ultralow threshold.¹⁰¹ Li *et al.* fabricated SiO₂ nanocones by nanosphere lithography, and then transferred and conformed a CVD-grown monolayer MoS₂ sheet onto the nanocones (Fig. 11(a)). With this process, a large biaxial strain was applied in MoS₂ on top of the nanocones, and the strain gradually decreases from the tip to the perimeter of the nanocones (Fig. 11(b)). It thus continuously modulated the bandgap of MoS₂ and created an optoelectronic crystal that consists of “artificial atoms” capable of broadband light absorption and efficient funneling of photo-generated excitons.¹⁰² Figure 11(c) shows that the PL peak of strained MoS₂ from A exciton apparently red-shifts, and the energy

difference between most strained MoS₂ and unstrained MoS₂ reaches up to 50 meV. Figure 11(d) shows a schematic of the funnel effect of “artificial atoms,” where photo-generated excitons drift in the potential from the perimeter towards the tip of the nanocone, and finally, the concentrated excitons give emission with a longer wavelength.

Modification of substrate surface is another optional way to modulate the properties of 2D overlayer semiconductors. *Ab initio* DFT calculations show that a defect-free SiO₂ substrate does not have significant influences on the electrical properties of MoS₂ monolayer due to weak interface interactions. However, if Na impurities and O dangling bonds are introduced onto the SiO₂ surface, the MoS₂ monolayer will be modulated from n- to p-type due to the localized states. It means that the conductivity of 2D semiconducting TMDs depends on the charge polarity of the traps at the substrate surface, as well as the energy-level alignment of the trap states within the bandgap of 2D TMDs.¹⁰³ Experimental results have shown that Na ions in a glass substrate can be driven by an E-field, creating a space charge doping of MoS₂ at the MoS₂/glass interface by the accumulation or depletion of Na ions. The induced n-doping density reaches up to $4 \times 10^{14} \text{ cm}^{-2}$ in few-layer MoS₂. With the increase in the carrier density, MoS₂ experiences an insulator to metal and finally to superconductor transition with the critical temperature at $\sim 10 \text{ K}$.¹⁰⁴ These results actually reveal possibilities of modulating the properties of 2D semiconductors by pre-modifying the same substrate with different methods, which might be more cost-effective compared to the modulation way through the alternation of substrates.

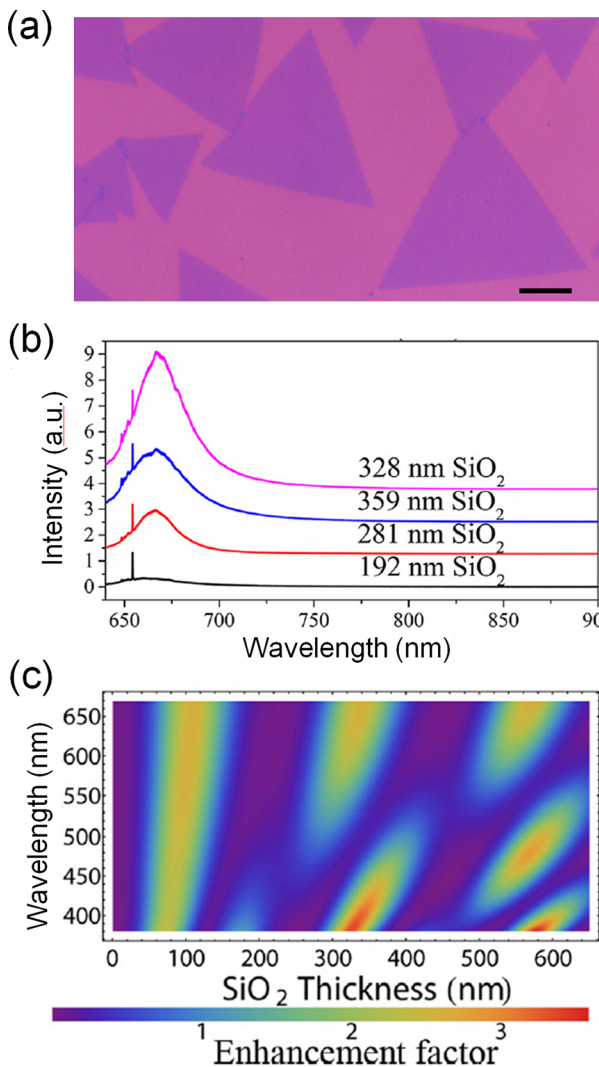


FIG. 10. (a) Monolayer MoS₂ grown by CVD. Scale bar, 10 μm . (b) Typical PL spectra of monolayer MoS₂ on SiO₂/Si substrates with different SiO₂ thicknesses. (c) The calculated contour plot of the total enhancement factor of the A exciton ($\sim 670 \text{ nm}$) emission of monolayer MoS₂ as a function of both SiO₂ thickness and excitation wavelength. Reprinted with permission from Zhang *et al.*, Appl. Phys. Lett. **107**, 101904 (2015). Copyright 2015 AIP Publishing LLC.

B. 2D materials as substrates

Usual substrates, including natural or grown crystals and deposited oxides, are subject to impurities, defects, and relatively large surface roughness. When 2D semiconductors are stacked on a substrate, impurities, defects, roughness, and surface phonons of the substrate could trap charges or scatter carriers at the 2D/substrate interface, reducing the carrier mobility and doping the 2D semiconductors away from their charge neutrality. As such, graphene devices on standard Si/SiO₂ substrates have carrier mobilities far less than their theoretical values.^{51,105–107} In this regard, 2D materials, owing to their atomic flatness and absence of dangling bonds or charge traps, are promising substrates for the devices with 2D semiconductors as channels. This concept has also become one of the basic points in the emerging van der Waals heterostructures.²¹ Many types of 2D heterostructures including graphene/TMDs and TMDs/TMDs have been

successfully fabricated or synthesized during the last several years.^{108–112} In these heterostructures, interface interactions are crucial for novel phenomena, such as ultrafast charge transfer¹⁰⁸ and spin-orbit interactions.^{111,112}

Insulating 2D materials, particularly hexagonal boron nitride (h-BN), are ideal dielectric substrates for 2D devices. h-BN is chemically inert owing to the strong, in-plane, and ionic bonding of the planar hexagonal lattice. Other benefits of h-BN include the superior mechanical strength¹¹³ and low dielectric screening.¹¹⁴ Dean *et al.* built graphene-based electronic devices on h-BN substrates through a mechanical transfer process.⁵² The monolayer and bilayer graphene devices on h-BN substrates have mobilities and carrier inhomogeneities that range from several times to almost an order of magnitude better than the devices on SiO₂. There is no change in the doping level of the graphene/h-BN devices after heating at a reducing atmosphere, suggesting a stable chemical reactivity, different from the devices on SiO₂.⁵² h-BN has also been employed as the dielectric substrate (or supporting layer) of 2D semiconductors, such as MoS₂. Lee *et al.* developed MoS₂-based FETs with h-BN as the gate dielectric and graphene as the gate electrode, by stacking the exfoliated 2D materials in sequence (Figs. 12(a) and 12(b)). Compared with the MoS₂ FET device on SiO₂ (MS), the devices of MoS₂ on h-BN (MB and MBG) show moderately high field-effect mobility, low operating gate voltage, and greatly reduced hysteresis in transfer curves (Figs. 12(c) and 12(d)). These devices with the key components composed of all 2D materials facilitate the fabrication of flexible electronic devices with unchanged performances under bending.¹¹⁵ The A_{1g} mode in Raman spectra of MoS₂ on h-BN shows a blue-shift and a narrower line width compared to that on SiO₂, suggesting a much less doping effect due to the much fewer charged impurities and defects.¹¹⁶ Ross *et al.* achieved lateral p–n junctions in monolayer WSe₂ by electrostatically gating with BN as the dielectric layer and multiple metal pads as back gate electrodes. Besides as a high-quality dielectric layer, BN also functions as a disorder-free substrate to minimize non-radiative energy relaxation pathways. Due to the effective injection of electrons and holes, the WSe₂/BN structure yields an electroluminescence with 1000 times smaller injection current and 10 times smaller linewidth than MoS₂-based structures.¹¹⁷

These benefits that h-BN brings to 2D electronics inspire researchers to synthesize h-BN flakes by chemical vapor deposition (CVD), which is superior to mechanical exfoliation in large flake size and mass production. Kim *et al.* synthesized large-scale, multilayer h-BN flakes by CVD on Fe foils with a borazine precursor.¹¹⁸ Other 2D materials, including graphene, MoS₂, and WSe₂, were also grown by CVD on different substrates. These 2D materials were then transferred onto a target substrate and built into FET devices consisting of 2D material (graphene, MoS₂, and WSe₂) channels on h-BN substrates. The mobilities were found to be improved by ~ 2 times for graphene devices and ~ 4 times for MoS₂ devices. Although the CVD synthesis of both BN and TMDs could enlarge the scale of devices, the interface between them might be contaminated or rippled during the transfer and stack process, which could reduce the coupling

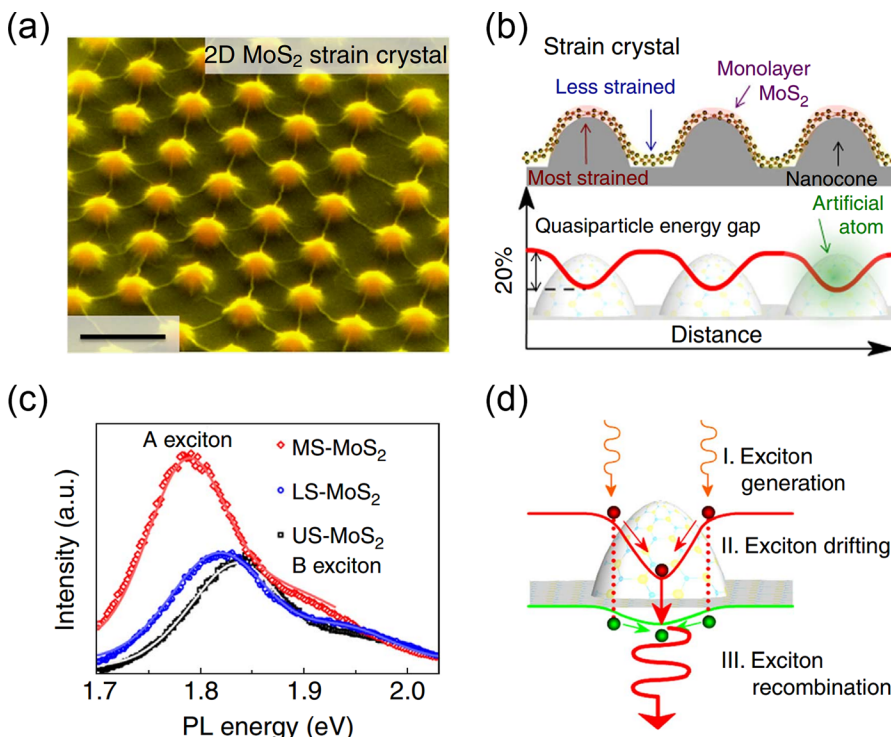


FIG. 11. (a) False-color SEM image of 2D strained MoS₂ crystal defined by the periodic SiO₂ nanocone array, forming “artificial atoms.” Scale bar, 500 nm. (b) Schematic of the strained MoS₂ conformed on SiO₂ nanocones. The energy bandgap of MoS₂ is spatially modulated and inversely follows the strain profile. (c) PL spectra of most strained-MoS₂ (MS-MoS₂), less strained-MoS₂ (LS-MoS₂), and unstrained MoS₂ (US-MoS₂). (d) Schematic of the funnel effect from an “artificial atom.” Reprinted with permission from Li *et al.*, Nat. Commun. **6**, 7381 (2015). Copyright 2015 Macmillan Publishers Limited.

at the interface and become an obstacle to higher performance of devices.

Direct synthesis of 2D semiconductors on h-BN substrates thus becomes an ideal technique to obtain a clean, strongly coupled 2D/h-BN interface. Yan *et al.* developed a CVD method to directly grow single- and few-layer MoS₂ on exfoliated high-quality h-BN flakes.¹¹⁹ The growth mechanism could be screw-dislocation driven or “layer by layer” depending on the different supersaturation condition of

precursors. Single-layer MoS₂ grown on h-BN was found to prefer low relative rotation angles (<5°) between the MoS₂ and h-BN lattices prevail. The as-grown MoS₂/h-BN shows a strong PL peak close to that of free-standing MoS₂ but different from that of MoS₂/SiO₂, suggesting that the as-grown MoS₂/h-BN has less perturbed electrical environment and is promising for high-quality MoS₂-based devices. Wang *et al.* realized an all-CVD growth of MoS₂/h-BN by a first-step CVD growth of h-BN film on copper, then a transfer of h-

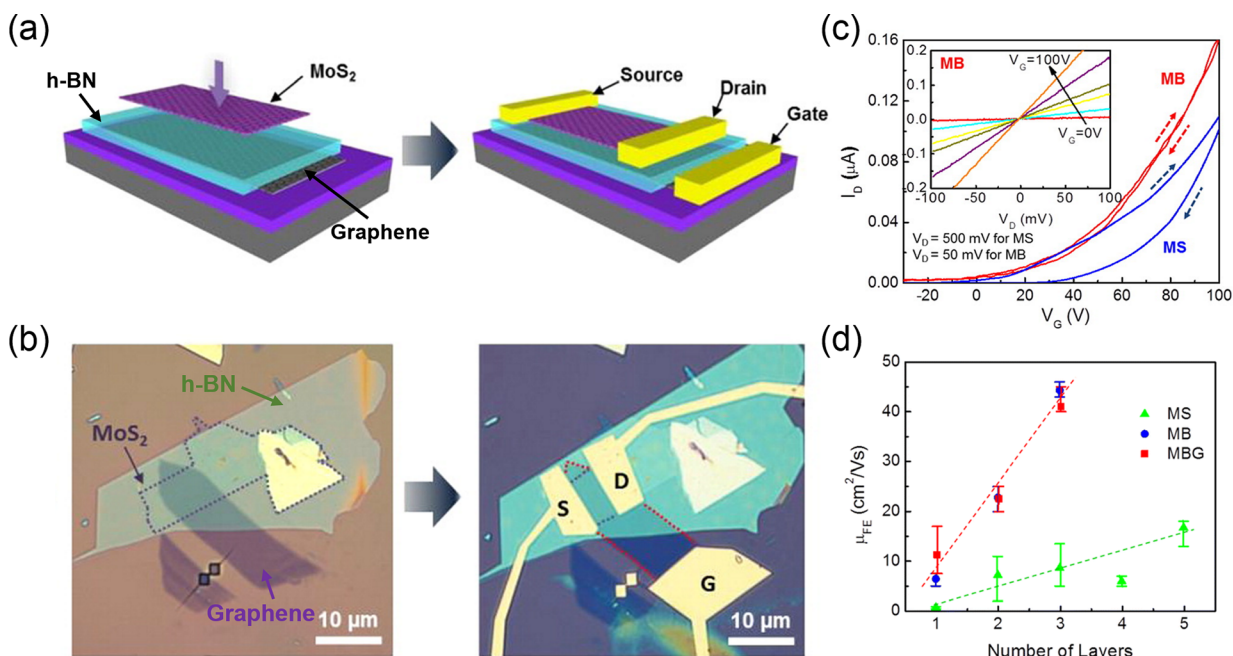


FIG. 12. (a) Schematic and (b) optical images of the stacked MoS₂/h-BN/graphene structure and device, where MoS₂ functions as the semiconducting channel, h-BN the dielectric layer, and graphene the back gate electrode. (c) Transfer curves of MoS₂ FET on SiO₂ (MS) and MoS₂ FET on SiO₂-supported h-BN (MB). (d) Dependence of carrier mobility on the number of layers for the MS device, MB device, and MoS₂/h-BN/graphene (MBG) device. Reprinted with permission from Lee *et al.*, ACS Nano **7**, 7931 (2013). Copyright 2013 American Chemical Society.

BN film on SiO_2/Si as a new substrate, and finally, a second-step CVD growth of MoS_2 on h-BN film.¹²⁰ Recently, Behura *et al.* demonstrated a direct *in-situ* growth of large-area, transfer-free TMDs/BN heterostructures by CVD.¹²¹ They first employed an oxide-assisted growth of large-area, continuous h-BN thin films on SiO_2/Si and quartz, and furthermore grew TMDs (MoS_2 and WS_2) on h-BN films. This growth method eliminates the need for metal catalysts, substrate loading/unloading, and post-synthesis transfer steps, resulting in a clean, unwrinkled interface between TMDs and h-BN. The heterostructures showed enhanced carrier mobility due to the reduction of scattering from roughness and charged impurities, which is verified by the increase in electrical conductivity.

C. “Active” substrates

Either the alternation, patterning, or doping of substrates, or the utilization of 2D substrates, is still a one-way other than a reversible approach for the modulation of 2D overlayer semiconductors, although these ways seem facile and straightforward. Reversible modulation of the properties of 2D semiconductors requires an “active” and reconfigurable substrate that offers switchable functionalities by the strong interaction between the substrate and the 2D overlayers. As substrates are indispensable in 2D semiconductor devices, the delicate selection of active substrates provides numerous possibilities to integrate novel functionalities into the 2D devices without introducing additional components. These are crucial for the next generation devices that require miniaturization, multiple functionalities, and intelligence.

Phase transition materials are good candidates as active substrates. In these materials, different phases could be switched on through the change of external stimuli, such as

temperature, pressure, electric field, or light. The utilization of phase transition materials as active substrates in 2D semiconductor devices requires these materials to be in both solid states before and after the phase transition at a moderate triggering condition. In this regard, vanadium dioxide (VO_2) is an intriguing option as it undergoes a thermally driven metal-insulator transition (MIT) at slightly above the room temperature (68°C).¹²² The MIT can also be triggered electrostatically under a strong electric field induced by ionic liquid gating.¹²³ As the MIT occurs, the physical properties of VO_2 , including band structures, optical indexes, lattice constants, and carrier densities, change abruptly and drastically.^{124–126} Figure 13(a) shows the apparent color change across the MIT of VO_2 as revealed by the optical images. If a monolayer 2D semiconductor is sitting on a VO_2 substrate, the ultrathin 2D material will be susceptible to the MIT of VO_2 . Recently, Hou *et al.* reported a modulation of PL of monolayer MoS_2 by interfacing it with VO_2 .¹²⁶ In their experiments, chemical-vapor-deposited MoS_2 monolayers were transferred onto pulsed-laser-deposited (PLD) VO_2 thin films on SiO_2/Si substrates (Fig. 13(a)).^{47,126} The PL of monolayer MoS_2 was found to be greatly enhanced at the specific thicknesses of VO_2 and SiO_2 they used, when the underlying VO_2 switched from the insulating to the metallic phase (Fig. 13(b)). Across the MIT of VO_2 , the spectral weight ratios of trions to excitons of MoS_2 are almost unchanged, and the PL enhancement still exists with an insertion of insulating boron nitride (BN) layers between MoS_2 and VO_2 (Fig. 13(c)). These results exclude strain, charge transfer, or dielectric screening effects, yet are attributed to the optical interference effect as the dominant mechanism. The reversible MIT of VO_2 with a hysteresis offers a memory effect that allows a rewritable PL pattern of MoS_2 by a precise control of the VO_2 phase with laser

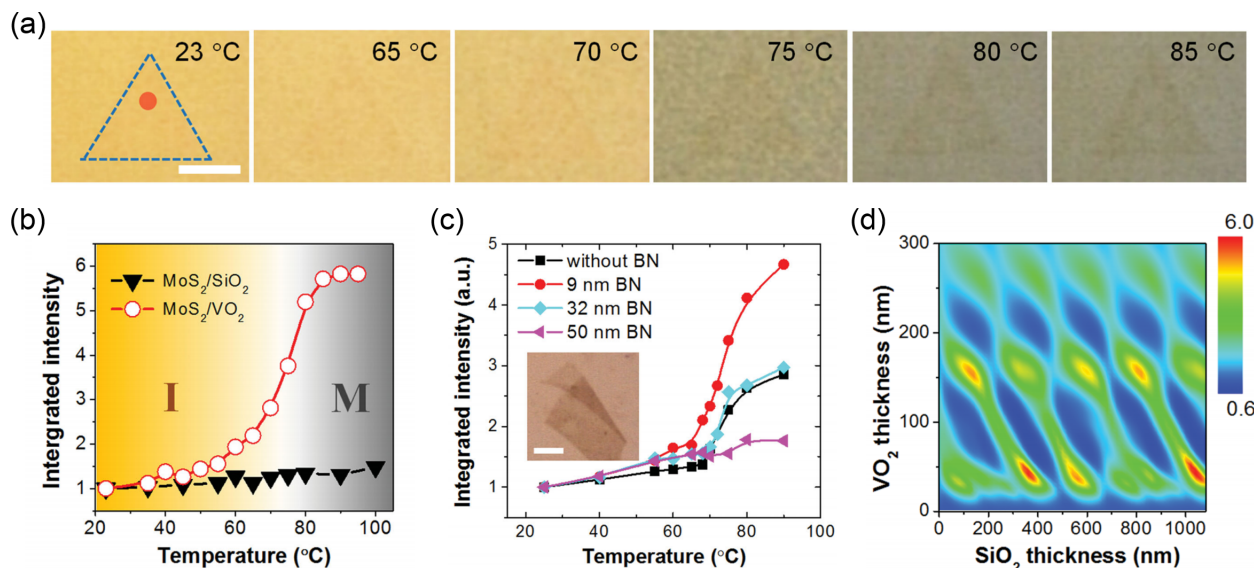


FIG. 13. (a) CVD-grown MoS_2 monolayer on a PLD VO_2 thin film at various temperatures across the phase transition of VO_2 . The dashed triangle highlights the outline of the MoS_2 monolayer and the red dot indicates the excitation laser spot for PL measurements. Scale bar, 5 μm . (b) Integrated PL intensity of MoS_2 on VO_2 versus that on SiO_2 . (c) PL intensities of MoS_2 without and with an insertion of variedly thick BN flakes between MoS_2 and VO_2 . The inset shows a BN flake that is supported by VO_2 (background) and covered by a monolayer MoS_2 (invisible); scale bar, 5 μm . (d) Contour of PL enhancement factors as functions of both VO_2 and SiO_2 thicknesses. The enhancement factor is defined as the ratio of the integrated intensity of the MoS_2 PL immediately after to that immediately before the phase transition of VO_2 . Reprinted with permission from Hou *et al.*, Small 12, 3976 (2016). Copyright 2016 Wiley-VCH Verlag GmbH & Co. KGaA, Weinheim.

writing, potentially providing applications in switches and sensors based on 2D semiconductors. As optical interference strongly depends on the pathway of light, the enhancement factor of MoS₂ PL is actually determined by both the thicknesses of MoS₂ and SiO₂, and in some cases, it is lower than 1 suggesting a weakening of PL across the MIT of VO₂ (Fig. 13(d)). This method thereby provides a controlled way to modulate the PL of MoS₂ as well as other 2D semiconductors, simply through an active substrate with a phase transition.¹²⁶

Ferroelectric materials, as another type of active materials, are also a good option to modulate the properties of 2D semiconductors. Ferroelectric materials have been studied for decades and involved in wide applications as they can reverse the spontaneous polarization controlled by electric fields.¹²⁷ The accompanied strain in ferroelectric material has been utilized to compress 2D semiconductors in a reversible way.¹²⁸ Ferroelectric field-effect transistor (FeFET), as a novel type of transistors with a ferroelectric material as the gate dielectric, has been a potential candidate for future memory devices.¹²⁹ 2D semiconductors have been exploited as the channel materials to build 2D/ferroelectric FETs or photodetectors.^{130–132} However, these devices are still subject to slow dipole dynamics, high operation voltage, or slow switching speed. To overcome these shortages, Ko *et al.* developed 2D/ferroelectric nonvolatile memory devices with 2D TMDs (n-type MoS₂ or p-type WSe₂) as the channel material and a PZT (Pb[Zr_{0.2}Ti_{0.8}]O₃) thin film as the dielectric layer (Figs. 14(a) and 14(b)).¹³³ These solid-state devices not only exhibit low switching voltages, high on–off ratios, and superior data retention in electrical transport (Figs. 14(c) and 14(d)), but also show a

nonvolatile optical memory effect in which the PL intensity of 2D semiconductors can be controlled reversibly through the ferroelectric gating (Figs. 14(e) and 14(f)). The PL peak height can be dynamically modulated with a factor up to ~7, by altering the polarization of the ferroelectric substrate between two states (P_{\uparrow} and P_{\downarrow} , Fig. 14(f)). This modulation effect might be further improved by introducing other ferroelectric materials with stronger polarization, such as BiFeO₃. It thus opens up new options for materials as active substrates to achieve the modulation of 2D semiconductors.¹³³

D. Flexible or stretchable substrates

Flexible or stretchable electronics has attracted intensive attention owing to great demands of foldable or wearable devices in recent decades.^{134,135} A secret to create flexible or stretchable devices is to make the key materials thin.¹³⁶ In this regard, 2D semiconductors are ideal as the key components in these devices because of the atomic thickness. Substrates should also be flexible or stretchable, and thus, elastic polymers are preferred. Most studies on flexible or stretchable devices of 2D materials are focused on their unchanged properties under bending, twisting, stretching, or compressing.^{63,137,138} However, as bandgaps of 2D semiconductors are usually sensitive to applied strain, these flexible or stretchable substrates also provide effective platforms to reversibly modulate the properties of 2D semiconductors, typically by the so-called strain engineering.¹³⁹

Strain engineered graphene has been predicted and verified to possess many interesting properties and applications.^{140–142} The first report of strain engineered MoS₂ by

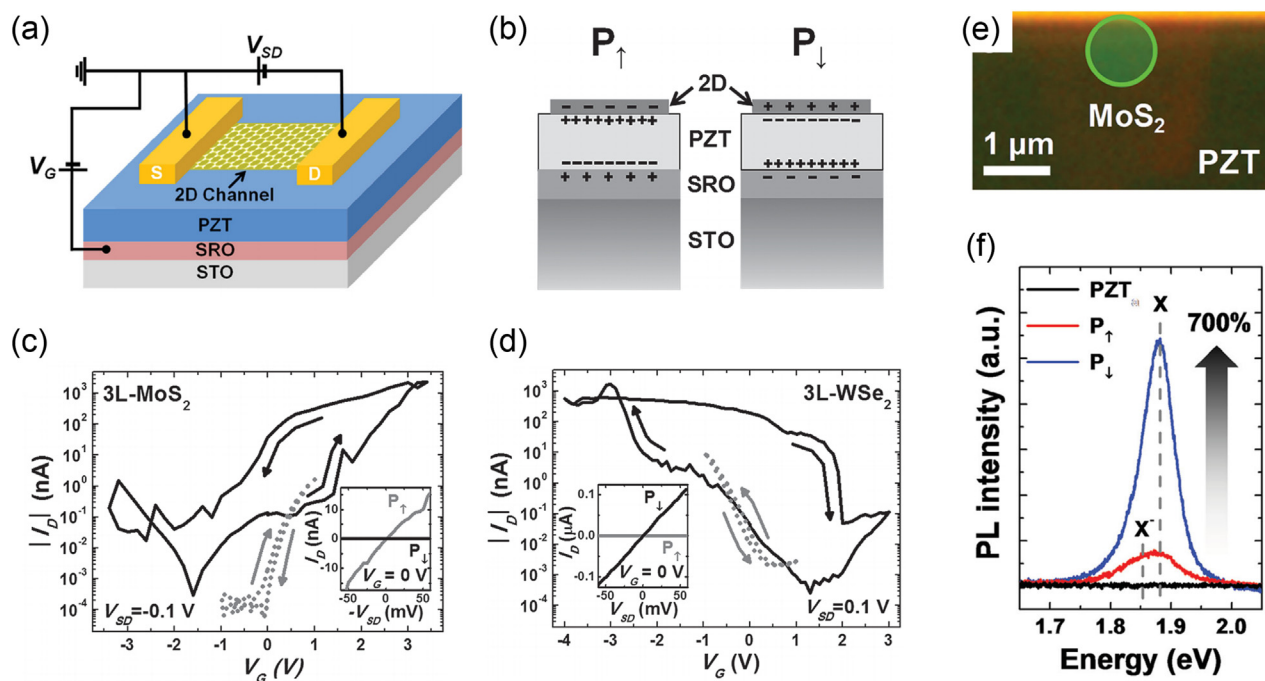


FIG. 14. (a) Schematic of a FeFET based on 2D TMDs/PZT heterostructures with a back gate configuration. (b) Schematic of the gating operation in the FeFET device for the up-polarized (P_{\uparrow}) and down-polarized (P_{\downarrow}) states at $V_G = 0$. Transfer curves of (c) n-type trilayer-MoS₂ and (d) p-type trilayer-WSe₂ based FeFET devices. Regular FET behavior of each device without ferroelectric poling is also shown in dashed lines. (e) Optical microscopy image of a MoS₂ monolayer on PZT from the green circle labelled in (e). Reprinted with permission from Ko *et al.*, Adv. Mater. **28**, 2923 (2016). Copyright 2016 Wiley-VCH Verlag GmbH & Co. KGaA, Weinheim.

flexible substrates (PC) has been discussed in Section II A of this review. Bending the substrates could quantitatively generate various tensile strains in the MoS₂ overlayer, thus decreasing the bandgap of MoS₂ and altering its photoluminescence,^{44,59} which reversibly modulates the properties of 2D semiconductors by the substrate-enabled strain engineering. Piezoelectricity of monolayer MoS₂ was achieved by cyclic stretching and releasing a polyethylene terephthalate (PET) flexible substrate. The strain-induced polarization charges produce oscillating electrical outputs and also modulate the charge carrier transport at the MoS₂-metal barrier.¹⁴³ Another approach to strain engineering of 2D semiconductors is to stretch or compress substrates. This process is also thoroughly reversible if the substrates are made of stretchable polymers. Wrinkles or ripples are usually created in this process and their geometries can be controlled by the pre-stretching of substrates.^{144–146}

Castellanos-Gomez *et al.* obtained wrinkled MoS₂ nanolayers by depositing mechanically exfoliated few-layer MoS₂ flakes onto a pre-stretched elastomeric substrate and then releasing the substrate (Fig. 15(a)).¹⁴⁴ The uniaxial strain in wrinkles red-shifts the PL peaks of MoS₂, suggesting a tensile strain there (Fig. 15(b)). The maximum tensile strain is accumulated at the apex of wrinkles, which reduces the bandgap of MoS₂ there and causes funneling of photo-generated excitons toward the apex (Fig. 15(c)). This result is very similar to that of patterned nanocones-conformed MoS₂ reported by Li *et al.*,¹⁰² as discussed at the beginning of Section III, although in the latter case the strain is biaxial and the substrate is rigid and not stretchable. Yang *et al.* utilized a similar pre-stretch/release process to make ReSe₂ wrinkles (Fig. 16(a)).¹⁴⁵ They also observed a red-shift of the PL peak and a funneling effect in ReSe₂ wrinkles (Fig.

16(b)). However, an interesting discovery is that magnetism appears on ReSe₂ wrinkles because spin polarization takes place locally at the strained regions, as revealed by both the magnetic force microscopy (MFM) measurements (Figs. 16(c) and 16(d)) and DFT calculations. The electrical conductivity can also be modulated by the geometry of ReSe₂ wrinkles that is controlled by different pre-strains (Fig. 16(e)). Quereda *et al.* studied the modulation of optical properties in ripples of multi-layer black phosphorus (BP).¹⁴⁶ In the regions of tensile and compressive stresses in BP ripples, they observed a remarkable difference in the optical bandgap of up to ~ 0.7 eV, which is much larger than the values reported in 2D TMDs. Theoretical modelling confirms this periodic stress modulation and predicts quantum confinement of carriers at low temperatures. It reveals a much higher sensitivity of BP band structures to strain compared to that of 2D TMDs, which could be utilized as an extraordinary candidate to create exciton funnels. These studies relevant to 2D TMDs and BP show that the substrate-enabled strain engineering can tune the physical properties of 2D semiconductors, thus providing wide applications including strain sensors, stretchable electrodes, and flexible electronics and photonics.

IV. PROSPECTIVES AND CHALLENGES

Since the properties of 2D semiconductors are susceptible to the substrate it lays on, the rational choice of the substrate type and the precise control of the interface are of vital importance. In recent years, researchers have already played with various 2D/substrate interfaces. As we summarized above, patterned substrates, 2D-material substrates with perfect atomic surfaces, active substrates with diverse functionalities, and flexible or stretchable substrates have been employed to modulate the properties of 2D semiconductors and design cooperative devices. In addition, some non-conventional concepts are explored and invoked to develop novel functionalities in 2D semiconductors. For example, the exchange proximity interaction has been theoretically predicted to induce a large spin splitting inside 2D materials when contacting with ferromagnets.^{147–149} Recent experimental work has realized this effect in ferromagnetic insulator/graphene heterostructures, including EuO/graphene¹⁵⁰ and EuS/graphene.¹⁵¹ The interplay between spin and pseudospins resulting from the strong spin-orbit coupling in TMDs has been reported.¹⁵² Although current theoretical and experimental work was mainly focused on the induced ferromagnetism in graphene, whether the proximity effect could induce valley polarization or “valley ferromagnetism” in the family of 2D semiconductors becomes an open question. Further extension of ferromagnetic insulator substrates to 2D semiconductors may lead to new routes for spin manipulation and novel spintronic applications. On the other hand, interplays of 2D semiconductors with various novel substrates, including superconductors, topological insulators, strong-correlated oxides, etc., are also intriguing topics in future as they will generate lots of emerging effects for the development of fantastic devices. The cooperative interaction of 2D semiconductors with these different

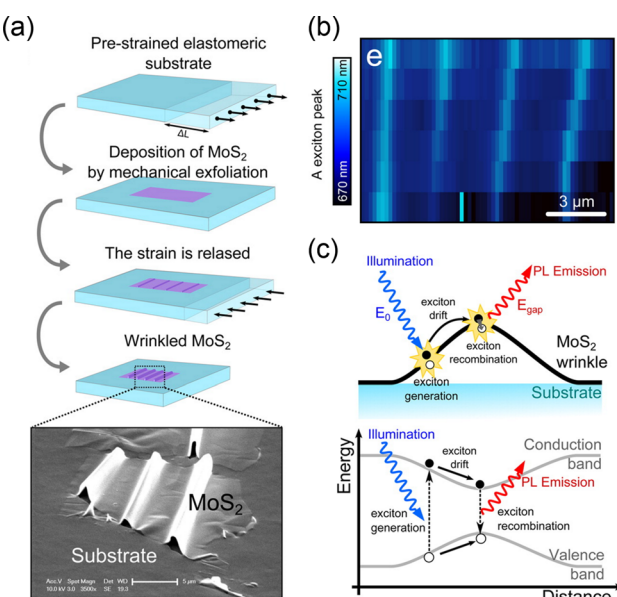


FIG. 15. (a) Schematic diagram of the fabrication process, and the as-fabricated sample, of MoS₂ wrinkles. (b) Mapping of the A exciton peak of a MoS₂ flake with four wrinkles. (c) Schematic diagram of the funnel effect in a MoS₂ wrinkle. Reprinted with permission from Castellanos-Gomez *et al.*, Nano Lett. **13**, 5361 (2013). Copyright 2013 American Chemical Society.

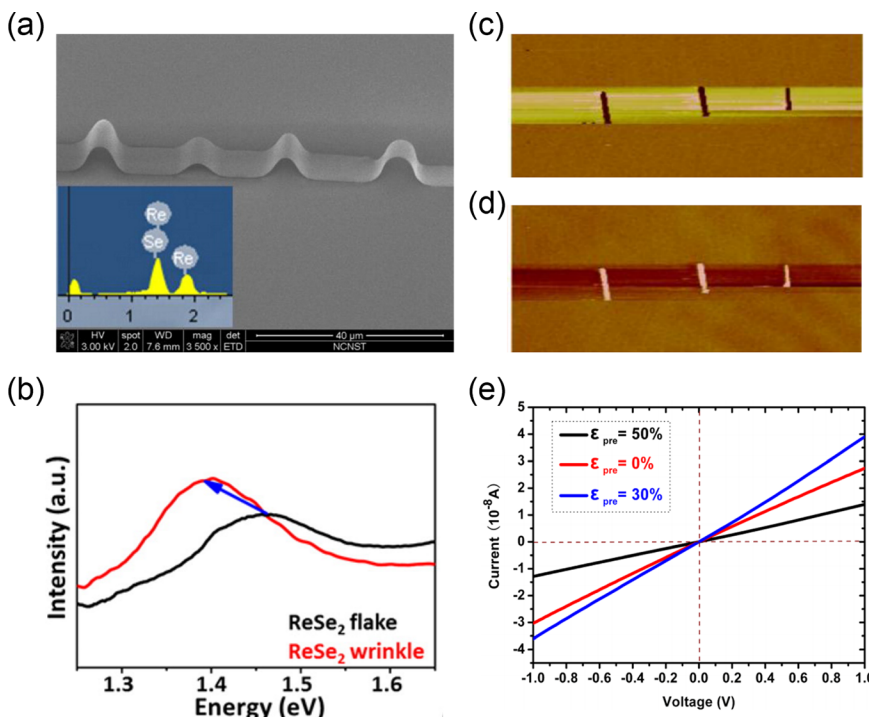


FIG. 16. (a) SEM image of wrinkled ReSe_2 . (b) PL spectra of the flat (black) and wrinkled (red) regions of the ReSe_2 monolayer as shown in (a). (c) MFM phase, and (d) MFM amplitude images of a wrinkled monolayer ReSe_2 . The reverse shifts in the phase and amplitude images suggest that the ReSe_2 becomes magnetic at the wrinkled (strained) regions. (e) I–V curves of a device of two terminal ReSe_2 wrinkle made by different pre-strains. Reprinted with permission from Yang *et al.*, *Nano Lett.* **15**, 1660 (2015). Copyright 2015 American Chemical Society.

materials will also bring new opportunities in different research fields.

Moreover, mechanisms of interactions between 2D semiconductors and substrates are usually complicated, and in many cases, they function mutually rather than solo. Strain, charge transfer, dielectric screening, and optical interference often coupled together to influence the properties of 2D semiconducting overlayers on many types of substrates, especially on complex substrates. This also causes difficulties in the precise control of interface interactions for 2D/substrate systems. As such, there are still challenges in designing precise and reliable techniques to engineer substrates for the modulation of properties of 2D semiconductors.

Another unclear question in this research field is the effect of substrates on novel 2D semiconductors such as BP and graphdiyne, although those effects on 2D TMDs have been investigated intensively. BP has attracted growing attention recently. It is a direct bandgap semiconductor regardless of the number of layers, while the bandgap varies with altering the number of layers. This difference in band structures compared with 2D TMDs may have BP modulated by substrates in different ways, but has yet to be studied comprehensively. The fabrication and performance of devices based on these studies will be a new playground for researchers.

Last, although several separate approaches of substrate engineering have been developed, systematic designs of substrate engineering for integrated electronic and optoelectronic devices are still lacking. Actually, substrate engineering can be extended to develop large-area 2D devices with complex functionalities. For instance, delicate patterning of substrates could deliver the overlayer 2D semiconductors with n-doping, p-doping, or metallic features, based on the variety of mechanisms (doping, strain, etc.) as we discussed in this review. This implies that a fully functional device, including metallic

electrodes and semiconducting channels, can be built up by facilely engineering the substrate. It is a great challenge but reveals an interesting frontier in designing novel integrated devices.

ACKNOWLEDGMENTS

This work was supported by the Thousand Youth Talents Program in China, National Natural Science Foundation of China (Grant Nos. 51602173 and 11604010), Fundamental Research Funds for the Central Universities (FRF-TP-15-097A1), and Open Research Fund Program of the State Key Laboratory of Low-Dimensional Quantum Physics (KF201603 and KF201611).

- ¹A. P. Ramirez, *J. Phys.: Condens. Matter* **9**, 8171 (1997).
- ²R. Ramesh and N. A. Spaldin, *Nat. Mater.* **6**, 21 (2007).
- ³M. L. Lee, E. A. Fitzgerald, M. T. Bulsara, M. T. Currie, and A. Lochtefeld, *J. Appl. Phys.* **97**, 011101 (2005).
- ⁴R. H. Baughman, A. A. Zakhidov, and W. A. de Heer, *Science* **297**, 787 (2002).
- ⁵Y. N. Xia, P. D. Yang, Y. G. Sun, Y. Y. Wu, B. Mayers, B. Gates, Y. D. Yin, F. Kim, and Y. Q. Yan, *Adv. Mater.* **15**, 353 (2003).
- ⁶A. P. Alivisatos, *Science* **271**, 933 (1996).
- ⁷A. K. Geim and K. S. Novoselov, *Nat. Mater.* **6**, 183 (2007).
- ⁸S. Z. Butler, S. M. Hollen, L. Y. Cao, Y. Cui, J. A. Gupta, H. R. Gutierrez, T. F. Heinz, S. S. Hong, J. X. Huang, A. F. Ismach, E. Johnston-Halperin, M. Kuno, V. V. Plashnitsa, R. D. Robinson, R. S. Ruoff, S. Salahuddin, J. Shan, L. Shi, M. G. Spencer, M. Terrones, W. Windl, and J. E. Goldberger, *ACS Nano* **7**, 2898 (2013).
- ⁹K. S. Novoselov, A. K. Geim, S. V. Morozov, D. Jiang, Y. Zhang, S. V. Dubonos, I. V. Grigorieva, and A. A. Firsov, *Science* **306**, 666 (2004).
- ¹⁰Y. B. Zhang, Y. W. Tan, H. L. Stormer, and P. Kim, *Nature* **438**, 201 (2005).
- ¹¹K. S. Novoselov, A. K. Geim, S. V. Morozov, D. Jiang, M. I. Katsnelson, I. V. Grigorieva, S. V. Dubonos, and A. A. Firsov, *Nature* **438**, 197 (2005).
- ¹²A. A. Balandin, S. Ghosh, W. Z. Bao, I. Calizo, D. Teweldebrhan, F. Miao, and C. N. Lau, *Nano Lett.* **8**, 902 (2008).

- ¹³C. Lee, X. D. Wei, J. W. Kysar, and J. Hone, *Science* **321**, 385 (2008).
- ¹⁴M. Y. Han, B. Ozilimaz, Y. B. Zhang, and P. Kim, *Phys. Rev. Lett.* **98**, 206805 (2007).
- ¹⁵K. F. Mak, C. Lee, J. Hone, J. Shan, and T. F. Heinz, *Phys. Rev. Lett.* **105**, 136805 (2010).
- ¹⁶A. Splendiani, L. Sun, Y. Zhang, T. Li, J. Kim, C.-Y. Chim, G. Galli, and F. Wang, *Nano Lett.* **10**, 1271 (2010).
- ¹⁷L. K. Li, Y. J. Yu, G. J. Ye, Q. Q. Ge, X. D. Ou, H. Wu, D. L. Feng, X. H. Chen, and Y. B. Zhang, *Nat. Nanotechnol.* **9**, 372 (2014).
- ¹⁸M. Naguib, M. Kurtoglu, V. Presser, J. Lu, J. J. Niu, M. Heon, L. Hultman, Y. Gogotsi, and M. W. Barsoum, *Adv. Mater.* **23**, 4248 (2011).
- ¹⁹G. X. Li, Y. L. Li, H. B. Liu, Y. B. Guo, Y. J. Li, and D. B. Zhu, *Chem. Commun.* **46**, 3256 (2010).
- ²⁰J. Kang, S. Tongay, J. Zhou, J. B. Li, and J. Q. Wu, *Appl. Phys. Lett.* **102**, 012111 (2013).
- ²¹A. K. Geim and I. V. Grigorieva, *Nature* **499**, 419 (2013).
- ²²B. Radisavljevic, A. Radenovic, J. Brivio, V. Giacometti, and A. Kis, *Nat. Nanotechnol.* **6**, 147 (2011).
- ²³G. Fiori, F. Bonaccorso, G. Iannaccone, T. Palacios, D. Neumaier, A. Seabaugh, S. K. Banerjee, and L. Colombo, *Nat. Nanotechnol.* **9**, 768 (2014).
- ²⁴D. Sarkar, X. Xie, W. Liu, W. Cao, J. Kang, Y. Gong, S. Kraemer, P. M. Ajayan, and K. Banerjee, *Nature* **526**, 91 (2015).
- ²⁵O. Lopez-Sanchez, D. Lembke, M. Kayci, A. Radenovic, and A. Kis, *Nat. Nanotechnol.* **8**, 497 (2013).
- ²⁶W. J. Yu, Y. Liu, H. Zhou, A. Yin, Z. Li, Y. Huang, and X. Duan, *Nat. Nanotechnol.* **8**, 952 (2013).
- ²⁷Q. H. Wang, K. Kalantar-Zadeh, A. Kis, J. N. Coleman, and M. S. Strano, *Nat. Nanotechnol.* **7**, 699 (2012).
- ²⁸Z. Yin, H. Li, H. Li, L. Jiang, Y. Shi, Y. Sun, G. Lu, Q. Zhang, X. Chen, and H. Zhang, *ACS Nano* **6**, 74 (2012).
- ²⁹M. M. Ugeda, A. J. Bradley, S. F. Shi, F. H. da Jornada, Y. Zhang, D. Y. Qiu, W. Ruan, S. K. Mo, Z. Hussain, Z. X. Shen, F. Wang, S. G. Louie, and M. F. Crommie, *Nat. Mater.* **13**, 1091 (2014).
- ³⁰Z. Ye, T. Cao, K. O'Brien, H. Zhu, X. Yin, Y. Wang, S. G. Louie, and X. Zhang, *Nature* **513**, 214 (2014).
- ³¹P. Rivera, J. R. Schaibley, A. M. Jones, J. S. Ross, S. Wu, G. Aivazian, P. Klement, K. Seyler, G. Clark, N. J. Ghimire, J. Yan, D. G. Mandrus, W. Yao, and X. Xu, *Nat. Commun.* **6**, 6242 (2015).
- ³²D. Xiao, G.-B. Liu, W. Feng, X. Xu, and W. Yao, *Phys. Rev. Lett.* **108**, 196802 (2012).
- ³³H. Zeng, J. Dai, W. Yao, D. Xiao, and X. Cui, *Nat. Nanotechnol.* **7**, 490 (2012).
- ³⁴K. F. Mak, K. He, J. Shan, and T. F. Heinz, *Nat. Nanotechnol.* **7**, 494 (2012).
- ³⁵A. Srivastava, M. Sidler, A. V. Allain, D. S. Lembke, A. Kis, and A. Imamoglu, *Nat. Nanotechnol.* **10**, 491 (2015).
- ³⁶M. Koperski, K. Nogajewski, A. Arora, V. Cherkez, P. Mallet, J. Y. Veuilien, J. Marcus, P. Kossacki, and M. Potemski, *Nat. Nanotechnol.* **10**, 503 (2015).
- ³⁷Y.-M. He, G. Clark, J. R. Schaibley, Y. He, M.-C. Chen, Y.-J. Wei, X. Ding, Q. Zhang, W. Yao, X. Xu, C.-Y. Lu, and J.-W. Pan, *Nat. Nanotechnol.* **10**, 497 (2015).
- ³⁸C. Chakraborty, L. Kinnischitzke, K. M. Goodfellow, R. Beams, and A. N. Vamivakas, *Nat. Nanotechnol.* **10**, 507 (2015).
- ³⁹K. F. Mak, K. He, C. Lee, G. H. Lee, J. Hone, T. F. Heinz, and J. Shan, *Nat. Mater.* **12**, 207 (2013).
- ⁴⁰Z. Li, S.-W. Chang, C.-C. Chen, and S. B. Cronin, *Nano Res.* **7**, 973 (2014).
- ⁴¹S. Tongay, J. Zhou, C. Ataca, J. Liu, J. S. Kang, T. S. Matthews, L. You, J. B. Li, J. C. Grossman, and J. Q. Wu, *Nano Lett.* **13**, 2831 (2013).
- ⁴²S. Mouri, Y. Miyauchi, and K. Matsuda, *Nano Lett.* **13**, 5944 (2013).
- ⁴³Y. Wang, J. Z. Ou, S. Balendhran, A. F. Chrimes, M. Mortazavi, D. D. Yao, M. R. Field, K. Latham, V. Bansal, J. R. Friend, S. Zhuiykov, N. V. Medhekar, M. S. Strano, and K. Kalantar-zadeh, *ACS Nano* **7**, 10083 (2013).
- ⁴⁴H. J. Conley, B. Wang, J. I. Ziegler, R. F. Haglund, Jr., S. T. Pantelides, and K. I. Bolotin, *Nano Lett.* **13**, 3626 (2013).
- ⁴⁵S. B. Desai, G. Seol, J. S. Kang, H. Fang, C. Battaglia, R. Kapadia, J. W. Ager, J. Guo, and A. Javey, *Nano Lett.* **14**, 4592 (2014).
- ⁴⁶Y. H. Sun, K. Liu, X. P. Hong, M. Chen, J. Kim, S. F. Shi, J. Q. Wu, A. Zettl, and F. Wang, *Nano Lett.* **14**, 5329 (2014).
- ⁴⁷K. Liu, Q. Yan, M. Chen, W. Fan, Y. Sun, J. Suh, D. Fu, S. Lee, J. Zhou, S. Tongay, J. Ji, J. B. Neaton, and J. Wu, *Nano Lett.* **14**, 5097 (2014).
- ⁴⁸N. Scheuschner, O. Ochedowski, A.-M. Kaulitz, R. Gillen, M. Schleberger, and J. Maultzsch, *Phys. Rev. B* **89**, 125406 (2014).
- ⁴⁹T. Jin, J. Kang, E. S. Kim, S. Lee, and C. Lee, *J. Appl. Phys.* **114**, 164509 (2013).
- ⁵⁰S. Y. Zhou, G. H. Gweon, A. V. Fedorov, P. N. First, W. A. De Heer, D. H. Lee, F. Guinea, A. H. Castro Neto, and A. Lanzara, *Nat. Mater.* **6**, 770 (2007).
- ⁵¹J.-H. Chen, C. Jang, S. Xiao, M. Ishigami, and M. S. Fuhrer, *Nat. Nanotechnol.* **3**, 206 (2008).
- ⁵²C. R. Dean, A. F. Young, I. Meric, C. Lee, L. Wang, S. Sorgenfrei, K. Watanabe, T. Taniguchi, P. Kim, K. L. Shepard, and J. Hone, *Nat. Nanotechnol.* **5**, 722 (2010).
- ⁵³W. Jin, P.-C. Yeh, N. Zaki, D. Zhang, J. T. Liou, J. T. Sadowski, A. Barinov, M. Yablonskikh, J. I. Dadap, P. Sutter, I. P. Herman, and R. M. Osgood, Jr., *Phys. Rev. B* **91**, 121409(R) (2015).
- ⁵⁴M. Buscema, G. A. Steele, H. S. J. van der Zant, and A. Castellanos-Gomez, *Nano Res.* **7**, 561 (2014).
- ⁵⁵Y. F. Yu, Y. L. Xu, C. Xu, Y. Q. Cai, L. Q. Su, Y. Zhang, Y. W. Zhang, K. Gundogdu, and L. Y. Cao, *Adv. Funct. Mater.* **26**, 4733 (2016).
- ⁵⁶D. Sercombe, S. Schwarz, O. Del Pozo-Zamudio, F. Liu, B. J. Robinson, E. A. Chekhovich, I. I. Tartakovskii, O. Kolosov, and A. I. Tartakovskii, *Sci. Rep.* **3**, 3489 (2013).
- ⁵⁷Y. Li, Z. Qi, M. Liu, Y. Wang, X. Cheng, G. Zhang, and L. Sheng, *Nanoscale* **6**, 15248 (2014).
- ⁵⁸Y. Lin, X. Ling, L. Yu, S. Huang, A. L. Hsu, Y.-H. Lee, J. Kong, M. S. Dresselhaus, and T. Palacios, *Nano Lett.* **14**, 5569 (2014).
- ⁵⁹C. R. Zhu, G. Wang, B. L. Liu, X. Marie, X. F. Qiao, X. Zhang, X. X. Wu, H. Fan, P. H. Tan, T. Amand, and B. Urbaszek, *Phys. Rev. B* **88**, 121301 (2013).
- ⁶⁰Y. Wang, Z. H. Ni, Z. X. Shen, H. M. Wang, and Y. H. Wu, *Appl. Phys. Lett.* **92**, 043121 (2008).
- ⁶¹S.-L. Li, H. Miyazaki, H. Song, H. Kuramochi, S. Nakaharai, and K. Tsukagoshi, *ACS Nano* **6**, 7381 (2012).
- ⁶²J. Pu, Y. Yomogida, K. K. Liu, L. J. Li, Y. Iwasa, and T. Takenobu, *Nano Lett.* **12**, 4013 (2012).
- ⁶³H. Y. Chang, S. X. Yang, J. H. Lee, L. Tao, W. S. Hwang, D. Jena, N. S. Lu, and D. Akinwande, *ACS Nano* **7**, 5446 (2013).
- ⁶⁴J. Yoon, W. Park, G. Y. Bae, Y. Kim, H. S. Jang, Y. Hyun, S. K. Lim, Y. H. Kahng, W. K. Hong, B. H. Lee, and H. C. Ko, *Small* **9**, 3295 (2013).
- ⁶⁵H. Pan and Y. W. Zhang, *J. Phys. Chem. C* **116**, 11752 (2012).
- ⁶⁶H. L. Shi, H. Pan, Y. W. Zhang, and B. I. Yakobson, *Phys. Rev. B* **87**, 155304 (2013).
- ⁶⁷P. Lu, X. J. Wu, W. L. Guo, and X. C. Zeng, *Phys. Chem. Chem. Phys.* **14**, 13035 (2012).
- ⁶⁸K. He, C. Poole, K. F. Mak, and J. Shan, *Nano Lett.* **13**, 2931 (2013).
- ⁶⁹C. Rice, R. J. Young, R. Zan, U. Bangert, D. Wolverson, T. Georgiou, R. Jalil, and K. S. Novoselov, *Phys. Rev. B* **87**, 081307(R) (2013).
- ⁷⁰Z. Liu, M. Amani, S. Najmaei, Q. Xu, X. Zou, W. Zhou, T. Yu, C. Qiu, A. G. Birdwell, F. J. Crowne, R. Vajtai, B. I. Yakobson, Z. Xia, M. Dubey, P. M. Ajayan, and J. Lou, *Nat. Commun.* **5**, 5246 (2014).
- ⁷¹M. Amani, M. L. Chin, A. L. Mazzoni, R. A. Burke, S. Najmaei, P. M. Ajayan, J. Lou, and M. Dubey, *Appl. Phys. Lett.* **104**, 203506 (2014).
- ⁷²Y. L. Wang, C. X. Cong, C. Y. Qiu, and T. Yu, *Small* **9**, 2857 (2013).
- ⁷³C. Gong, C. Huang, J. Miller, L. Cheng, Y. Hao, D. Cobden, J. Kim, R. S. Ruoff, R. M. Wallace, K. Cho, X. Xu, and Y. J. Chabal, *ACS Nano* **7**, 11350 (2013).
- ⁷⁴C. Lee, H. Yan, L. E. Brus, T. F. Heinz, J. Hone, and S. Ryu, *ACS Nano* **4**, 2695 (2010).
- ⁷⁵H. Li, Q. Zhang, C. C. R. Yap, B. K. Tay, T. H. T. Edwin, A. Olivier, and D. Baillargeat, *Adv. Funct. Mater.* **22**, 1385 (2012).
- ⁷⁶B. J. Robinson, C. E. Giusca, Y. T. Gonzalez, N. D. Kay, O. Kazakova, and O. V. Kolosov, *2D Mater.* **2**, 015005 (2015).
- ⁷⁷H. Shi, R. Yan, S. Bertolazzi, J. Brivio, B. Gao, A. Kis, D. Jena, H. G. Xing, and L. Huang, *ACS Nano* **7**, 1072 (2013).
- ⁷⁸N. Peimyoo, W. H. Yang, J. Z. Shang, X. N. Shen, Y. L. Wang, and T. Yu, *ACS Nano* **8**, 11320 (2014).
- ⁷⁹H. Wang, C. Zhang, and F. Rana, *Nano Lett.* **15**, 339 (2015).
- ⁸⁰N. D. Kay, B. J. Robinson, V. I. Fal'ko, K. S. Novoselov, and O. V. Kolosov, *Nano Lett.* **14**, 3400 (2014).
- ⁸¹A. Castellanos-Gomez, M. Poot, G. A. Steele, H. S. J. van der Zant, N. Agrait, and G. Rubio-Bollinger, *Adv. Mater.* **24**, 772 (2012).
- ⁸²D. Jena and A. Konar, *Phys. Rev. Lett.* **98**, 136805 (2007).
- ⁸³L. V. Keldysh, *Phys. Status Solidi A* **164**, 3 (1997).
- ⁸⁴E. A. Muljarov, E. A. Zhukov, V. S. Dneprovskii, and Y. Masumoto, *Phys. Rev. B* **62**, 7420 (2000).
- ⁸⁵G. Goldoni, F. Rossi, and E. Molinari, *Phys. Rev. Lett.* **80**, 4995 (1998).

- ⁸⁶M. Kumagai and T. Takagahara, *Phys. Rev. B* **40**, 12359 (1989).
- ⁸⁷V. Perebeinos, J. Tersoff, and P. Avouris, *Phys. Rev. Lett.* **92**, 257402 (2004).
- ⁸⁸A. G. Walsh, A. N. Vamivakas, Y. Yin, S. B. Cronin, M. S. Unlu, B. B. Goldberg, and A. K. Swan, *Physica E* **40**, 2375 (2008).
- ⁸⁹F. Chen, J. Xia, D. K. Ferry, and N. Tao, *Nano Lett.* **9**, 2571 (2009).
- ⁹⁰A. K. M. Newaz, Y. S. Puzyrev, B. Wang, S. T. Pantelides, and K. I. Bolotin, *Nat. Commun.* **3**, 734 (2012).
- ⁹¹A. Chernikov, T. C. Berkelbach, H. M. Hill, A. Rigos, Y. L. Li, O. B. Aslan, D. R. Reichman, M. S. Hybertsen, and T. F. Heinz, *Phys. Rev. Lett.* **113**, 076802 (2014).
- ⁹²A. V. Stier, N. P. Wilson, G. Clark, X. D. Xu, and S. A. Crooker, *Nano Lett.* **16**, 7054 (2016).
- ⁹³K. Kaasbjerg, K. S. Thygesen, and K. W. Jacobsen, *Phys. Rev. B* **85**, 115317 (2012).
- ⁹⁴Z. H. Yu, Z. Y. Ong, Y. M. Pan, Y. Cui, R. Xin, Y. Shi, B. G. Wang, Y. Wu, T. S. Chen, Y. W. Zhang, G. Zhang, and X. R. Wang, *Adv. Mater.* **28**, 547 (2016).
- ⁹⁵L. Zeng, Z. Xin, S. W. Chen, G. Du, J. F. Kang, and X. Y. Liu, *Appl. Phys. Lett.* **103**, 113505 (2013).
- ⁹⁶C. F. Chen, C. H. Park, B. W. Boudouris, J. Horng, B. S. Geng, C. Girit, A. Zettl, M. F. Crommie, R. A. Segalman, S. G. Louie, and F. Wang, *Nature* **471**, 617 (2011).
- ⁹⁷J. Horng, C. F. Chen, B. S. Geng, C. Girit, Y. B. Zhang, Z. Hao, H. A. Bechtel, M. Martin, A. Zettl, M. F. Crommie, Y. R. Shen, and F. Wang, *Phys. Rev. B* **83**, 165113 (2011).
- ⁹⁸C. Casiraghi, A. Hartschuh, E. Lidorikis, H. Qian, H. Harutyunyan, T. Goksu, K. S. Novoselov, and A. C. Ferrari, *Nano Lett.* **7**, 2711 (2007).
- ⁹⁹D. Yoon, H. Moon, Y. W. Son, J. S. Choi, B. H. Park, Y. H. Cha, Y. D. Kim, and H. Cheong, *Phys. Rev. B* **80**, 125422 (2009).
- ¹⁰⁰H. Zhang, Y. Wan, Y. Ma, W. Wang, Y. Wang, and L. Dai, *Appl. Phys. Lett.* **107**, 101904 (2015).
- ¹⁰¹S. Wu, S. Buckley, J. R. Schaibley, L. Feng, J. Yan, D. G. Mandrus, F. Hatami, W. Yao, J. Vuckovic, A. Majumdar, and X. Xu, *Nature* **520**, 69 (2015).
- ¹⁰²H. Li, A. W. Contryman, X. Qian, S. M. Ardashani, Y. Gong, X. Wang, J. M. Weisse, C. H. Lee, J. Zhao, P. M. Ajayan, J. Li, H. C. Manoharan, and X. Zheng, *Nat. Commun.* **6**, 7381 (2015).
- ¹⁰³K. Dolui, I. Rungger, and S. Sanvito, *Phys. Rev. B* **87**, 165402 (2013).
- ¹⁰⁴J. Biscaras, Z. S. Chen, A. Paradisi, and A. Shukla, *Nat. Commun.* **6**, 8826 (2015).
- ¹⁰⁵T. Ando, *J. Phys. Soc. Jpn.* **75**, 124701 (2006).
- ¹⁰⁶E. H. Hwang, S. Adam, and S. Das Sarma, *Phys. Rev. Lett.* **98**, 186806 (2007).
- ¹⁰⁷S. V. Morozov, K. S. Novoselov, M. I. Katsnelson, F. Schedin, D. C. Elias, J. A. Jaszczak, and A. K. Geim, *Phys. Rev. Lett.* **100**, 016602 (2008).
- ¹⁰⁸X. P. Hong, J. Kim, S. F. Shi, Y. Zhang, C. H. Jin, Y. H. Sun, S. Tongay, J. Q. Wu, Y. F. Zhang, and F. Wang, *Nat. Nanotechnol.* **9**, 682 (2014).
- ¹⁰⁹Y. J. Gong, J. H. Lin, X. L. Wang, G. Shi, S. D. Lei, Z. Lin, X. L. Zou, G. L. Ye, R. Vajtai, B. I. Yakobson, H. Terrones, M. Terrones, B. K. Tay, J. Lou, S. T. Pantelides, Z. Liu, W. Zhou, and P. M. Ajayan, *Nat. Mater.* **13**, 1135 (2014).
- ¹¹⁰C. M. Huang, S. F. Wu, A. M. Sanchez, J. J. P. Peters, R. Beanland, J. S. Ross, P. Rivera, W. Yao, D. H. Cobden, and X. D. Xu, *Nat. Mater.* **13**, 1096 (2014).
- ¹¹¹Z. Wang, D. K. Ki, H. Chen, H. Berger, A. H. MacDonald, and A. F. Morpurgo, *Nat. Commun.* **6**, 8339 (2015).
- ¹¹²A. Avsar, J. Y. Tan, T. Taychatanapat, J. Balakrishnan, G. K. W. Koon, Y. Yeo, J. Lahiri, A. Carvalho, A. S. Rodin, E. C. T. O'Farrell, G. Eda, A. H. C. Neto, and B. Ozilmez, *Nat. Commun.* **5**, 4875 (2014).
- ¹¹³L. Song, L. J. Ci, H. Lu, P. B. Sorokin, C. H. Jin, J. Ni, A. G. Kvashnin, D. G. Kvashnin, J. Lou, B. I. Yakobson, and P. M. Ajayan, *Nano Lett.* **10**, 3209 (2010).
- ¹¹⁴F. Forster, A. Molina-Sanchez, S. Engels, A. Epping, K. Watanabe, T. Taniguchi, L. Wirtz, and C. Stampfer, *Phys. Rev. B* **88**, 085419 (2013).
- ¹¹⁵G. H. Lee, Y. J. Yu, X. Cui, N. Petrone, C. H. Lee, M. S. Choi, D. Y. Lee, C. Lee, W. J. Yoo, K. Watanabe, T. Taniguchi, C. Nuckolls, P. Kim, and J. Hone, *ACS Nano* **7**, 7931 (2013).
- ¹¹⁶L. Li, I. Lee, D. Lim, M. Kang, G.-H. Kim, N. Aoki, Y. Ochiai, K. Watanabe, and T. Taniguchi, *Nanotechnology* **26**, 295702 (2015).
- ¹¹⁷J. S. Ross, P. Klement, A. M. Jones, N. J. Ghimire, J. Q. Yan, D. G. Mandrus, T. Taniguchi, K. Watanabe, K. Kitamura, W. Yao, D. H. Cobden, and X. D. Xu, *Nat. Nanotechnol.* **9**, 268 (2014).
- ¹¹⁸S. M. Kim, A. Hsu, M. H. Park, S. H. Chae, S. J. Yun, J. S. Lee, D. H. Cho, W. J. Fang, C. Lee, T. Palacios, M. Dresselhaus, K. K. Kim, Y. H. Lee, and J. Kong, *Nat. Commun.* **6**, 8662 (2015).
- ¹¹⁹A. M. Yan, J. Velasco, S. Kahn, K. Watanabe, T. Taniguchi, F. Wang, M. F. Crommie, and A. Zettl, *Nano Lett.* **15**, 6324 (2015).
- ¹²⁰S. S. Wang, X. C. Wang, and J. H. Warner, *ACS Nano* **9**, 5246 (2015).
- ¹²¹S. Behura, P. Nguyen, S. W. Che, R. Debbarma, and V. Berry, *J. Am. Chem. Soc.* **137**, 13060 (2015).
- ¹²²J. Cao, E. Ertekin, V. Srinivasan, W. Fan, S. Huang, H. Zheng, J. W. L. Yim, D. R. Khanal, D. F. Ogletree, J. C. Grossman, and J. Wu, *Nat. Nanotechnol.* **4**, 732 (2009).
- ¹²³K. Liu, D. Y. Fu, J. B. Cao, J. Suh, K. X. Wang, C. Cheng, D. F. Ogletree, H. Guo, S. Sengupta, A. Khan, C. W. Yeung, S. Salahuddin, M. M. Deshmukh, and J. Q. Wu, *Nano Lett.* **12**, 6272 (2012).
- ¹²⁴D. Y. Fu, K. Liu, T. Tao, K. Lo, C. Cheng, B. Liu, R. Zhang, H. A. Bechtel, and J. Q. Wu, *J. Appl. Phys.* **113**, 043707 (2013).
- ¹²⁵K. Liu, C. Cheng, Z. T. Cheng, K. V. Wang, R. Ramesh, and J. Q. Wu, *Nano Lett.* **12**, 6302 (2012).
- ¹²⁶J. Hou, X. Wang, D. Fu, C. Ko, Y. Chen, Y. Sun, S. Lee, K. X. Wang, K. Dong, Y. Sun, S. Tongay, L. Jiao, J. Yao, K. Liu, and J. Wu, *Small* **12**, 3976 (2016).
- ¹²⁷D. Damjanovic, *Rep. Prog. Phys.* **61**, 1267 (1998).
- ¹²⁸Y. Y. Hui, X. F. Liu, W. J. Jie, N. Y. Chan, J. H. Hao, Y. T. Hsu, L. J. Li, W. L. Guo, and S. P. Lau, *ACS Nano* **7**, 7126 (2013).
- ¹²⁹S. Mathews, R. Ramesh, T. Venkatesan, and J. Benedetto, *Science* **276**, 238 (1997).
- ¹³⁰A. Lipatov, P. Sharma, A. Gruverman, and A. Sinitskii, *ACS Nano* **9**, 8089 (2015).
- ¹³¹X. D. Wang, P. Wang, J. L. Wang, W. D. Hu, X. H. Zhou, N. Guo, H. Huang, S. Sun, H. Shen, T. Lin, M. H. Tang, L. Liao, A. Q. Jiang, J. L. Sun, X. J. Meng, X. S. Chen, W. Lu, and J. H. Chu, *Adv. Mater.* **27**, 6575 (2015).
- ¹³²Y. T. Lee, H. Kwon, J. S. Kim, H. H. Kim, Y. J. Lee, J. A. Lim, Y. W. Song, Y. Yi, W. K. Choi, D. K. Hwang, and S. Im, *ACS Nano* **9**, 10394 (2015).
- ¹³³C. Ko, Y. Lee, Y. Chen, J. Suh, D. Fu, A. Suslu, S. Lee, J. D. Clarkson, H. S. Choe, S. Tongay, R. Ramesh, and J. Wu, *Adv. Mater.* **28**, 2923 (2016).
- ¹³⁴Y. G. Sun and J. A. Rogers, *Adv. Mater.* **19**, 1897 (2007).
- ¹³⁵J. A. Rogers, T. Someya, and Y. G. Huang, *Science* **327**, 1603 (2010).
- ¹³⁶J. A. Rogers, M. G. Lagally, and R. G. Nuzzo, *Nature* **477**, 45 (2011).
- ¹³⁷D. Akinwande, N. Petrone, and J. Hone, *Nat. Commun.* **5**, 5678 (2014).
- ¹³⁸Y. Gao, Z. Liu, D.-M. Sun, L. Huang, L.-P. Ma, L.-C. Yin, T. Ma, Z. Zhang, X.-L. Ma, L.-M. Peng, H.-M. Cheng, and W. Ren, *Nat. Commun.* **6**, 8569 (2015).
- ¹³⁹R. Roldan, A. Castellanos-Gomez, E. Cappelluti, and F. Guinea, *J. Phys.: Condens. Matter* **27**, 313201 (2015).
- ¹⁴⁰F. Guinea, M. I. Katsnelson, and A. K. Geim, *Nat. Phys.* **6**, 30 (2010).
- ¹⁴¹G. Gui, J. Li, and J. X. Zhong, *Phys. Rev. B* **78**, 075435 (2008).
- ¹⁴²V. M. Pereira and A. H. Castro Neto, *Phys. Rev. Lett.* **103**, 046801 (2009).
- ¹⁴³W. Wu, L. Wang, Y. Li, F. Zhang, L. Lin, S. Niu, D. Chenet, X. Zhang, Y. Hao, T. F. Heinz, J. Hone, and Z. L. Wang, *Nature* **514**, 470 (2014).
- ¹⁴⁴A. Castellanos-Gomez, R. Roldan, E. Cappelluti, M. Buscema, F. Guinea, H. S. J. van der Zant, and G. A. Steele, *Nano Lett.* **13**, 5361 (2013).
- ¹⁴⁵S. X. Yang, C. Wang, H. Sahin, H. Chen, Y. Li, S. S. Li, A. Suslu, F. M. Peeters, Q. Liu, J. B. Li, and S. Tongay, *Nano Lett.* **15**, 1660 (2015).
- ¹⁴⁶J. Quereda, P. San-Jose, V. Parente, L. Vaquero-Garzon, A. J. Molina-Mendoza, N. Agrait, G. Rubio-Bollinger, F. Guinea, R. Roldan, and A. Castellanos-Gomez, *Nano Lett.* **16**, 2931 (2016).
- ¹⁴⁷H. Haugen, D. Huertas-Hernando, and A. Brataas, *Phys. Rev. B* **77**, 115406 (2008).
- ¹⁴⁸P. Lazic, K. D. Belashchenko, and I. Zutic, *Phys. Rev. B* **93**, 241401 (2016).
- ¹⁴⁹H. X. Yang, A. Hallal, D. Terrade, X. Waiental, S. Roche, and M. Chshiev, *Phys. Rev. Lett.* **110**, 046603 (2013).
- ¹⁵⁰A. G. Swartz, P. M. Odenthal, Y. F. Hao, R. S. Ruoff, and R. K. Kawakami, *ACS Nano* **6**, 10063 (2012).
- ¹⁵¹P. Wei, S. Lee, F. Lemaitre, L. Pinel, D. Cutaia, W. Cha, F. Katmis, Y. Zhu, D. Heiman, J. Hone, J. S. Moodera, and C. T. Chen, *Nat. Mater.* **15**, 711 (2016).
- ¹⁵²X. D. Xu, W. Yao, D. Xiao, and T. F. Heinz, *Nat. Phys.* **10**, 343 (2014).